Anharmonic Correction to Adsorption Free Energy from DFT-based MD using Thermodynamic Integration

Jonas Amsler,[*,†] Philipp N. Plessow,[†] Felix Studt,[†,‡] and Tomáš Bučko[*,¶,§]

†*Institute of Catalysis Research and Technology, Karlsruhe Institute of Technology, Hermann-von-Helmholtz-Platz 1, 76344 Eggenstein-Leopoldshafen, Germany*

‡*Institute for Chemical Technology and Polymer Chemistry, Karlsruhe Institute of Technology, Kaiserstr. 12, 76131 Karlsruhe, Germany*

¶*Department of Physical and Theoretical Chemistry, Faculty of Natural Sciences, Comenius University in Bratislava, Ilkovičova 6, SK-84215 Bratislava, Slovakia*

§*Institute of Inorganic Chemistry, Slovak Academy of Sciences, Dúbravská cesta 9, SK-84236 Bratislava, Slovakia*

E-mail: jonas.amsler@kit.edu; bucko19@uniba.sk

Abstract

Adsorption processes are often governed by weak interactions for which the estimate of entropy contributions by means of the harmonic approximation is prone to be inaccurate. Thermodynamic integration (TI) from the harmonic to the fully interacting system (λ-path integration) can be used to compute anharmonic corrections. Here we combine TI with (curvilinear) internal coordinates in periodic systems to make the formalism available in computational studies. Our implementation of ab initio molecular dynamics in VASP is independent of the reaction path and can thus be applied to study adsorption processes relative to the gas phase and does hence provide a useful

1

tool for computational catalysis. We discuss the approach in three model systems for which exact semi-analytical solutions exist and illustrate and quantify the importance of anharmonic vibrations, hindered rotations and hindered translations (dissociation). Eventually, we apply the method to study the adsorption of small particles in a zeolite (H-SSZ-13).

1 Introduction

The free energy of a system has contributions from both its enthalpy and entropy. Hence both contributions need to be considered in order to accurately calculate changes in free energies. An accurate description of entropy changes is particularly important for adsorption and desorption processes, as these often occur with a large loss (or gain) of entropy for an adsorbate. Adsorption steps are key for many important processes, e.g., they are essential for heterogeneous catalysis where the interaction of a solid catalyst with a gas-phase molecule is at the core of its function.[1] Unfortunately, the accurate treatment of entropy changes during these processes is also very challenging and typically approximated by consideration of harmonic potentials for the adsorbed system.

However, weakly interacting adsorbates often exhibit anharmonic degrees of freedom such as dissociation (translation) and rotation which are extremely poorly described[2–4] by the most popular and conceptually simple harmonic approximation.[5] Moreover, this stationary approach and its refinements on the global minimum (lattice gas, 2D ideal gas,[6] as well as interpolations in between[7–10] and descriptors based on confinement[11]) do neither consider adjacent local minima nor multiple adsorption sites.[12] Little advances have been achieved to properly account for adsorption entropy beyond the harmonic approximation although its necessity has been demonstrated for adsorption on metal surfaces and at acidic centers of zeolites.[13,14] In fact, recent computational studies indicate that there can be large deviations in the prediction of adsorption free energies, as it has been shown, e.g., for ethanol adsorption in zeolites.[14,15] Several strategies have evolved over the past years to tackle

these problems. ~~Sauer and coworkers have developed an anharmonic approximation around the stationary approach using multiple finite differences leading to anharmonic vibrational partition functions.[14,16–20]~~ By identification and separate treatment of the most important anharmonic degrees of freedom some approaches attempt to improve the accuracy of the static approach, where the thermodynamics of the system are deduced from the properties of the potential energy surface in vicinity to the stationary state of interest. For hindered rotational motion, for instance, potential energy models of different complexity (ranging from a single goniometric function up to explicitly sampled energy profiles) are used in classical,[21–23] semi-classical,[21–23] or quantum-mechanical[24] treatment and similar models exist also for hindered translations.[22] Nonetheless, the reliability of these approaches depends strongly on the particular thermodynamic conditions considered in the simulation. An elegant demonstration of this problem has been provided in a recent study of Jørgensen and Grönbeck, where predictions of harmonic, hindered, and free translator approximations in calculation of the entropy of CO and O adsorbed on Pt(111) have been tested against the complete potential energy sampling approach and experiments.[25] In the latter work, it was clearly shown that none of the simple approximations provides reliable predictions over a wide range of temperatures. Perhaps the most sophisticated correction to the static approach has been developed by Sauer and coworkers in which anharmonic vibrational partition functions have been determined by solving 1D Schrödinger equations defined for the potential energies explicitly sampled along individual vibrational eigenmodes expressed in terms of internal coordinates.[14,16–20] According to Piccini and Sauer, anharmonic contributions stabilize ethanol in H-MFI zeolite by $13\,\text{kJ}\,\text{mol}^{-1}$ at $300\,\text{K}$ ($20\,\text{kJ}\,\text{mol}^{-1}$ at $400\,\text{K}$).[14] Using a quasi-harmonic approximation (QHA) for ethanol adsorption in H-ZSM5 zeolite Alexopoulos et al. claim the traditional harmonic approximation overestimates adsorption free energies by $20\,\text{kJ}\,\text{mol}^{-1}$ to $50\,\text{kJ}\,\text{mol}^{-1}$.[15] The QHA relies on a vibrational density of states from molecular dynamics (MD), thereby taking into account raised temperature and the average of adjacent local minima. To date, accurate theoretical (but also experimental) reports on

adsorption free energies are rare mostly in lack of accurate accounts for entropy. Even simple internal rotations in n-alkanes are incorrectly described by the harmonic approximation and have therefore been subject to numerous investigations.[26–28]

MD simulations, typically based on density functional theory (DFT), in combination with enhanced sampling techniques can be used to determine changes in entropy beyond the harmonic approximation. Inherently, established methods like Blue Moon[29,30] or Umbrella[31–33] sampling require the integration over a numerical descriptor for the reaction path called collective variable (CV) or reaction coordinate ξ. The major attention of these tools in heterogeneous catalysis[3,4,34–38] has been paid to surface reaction steps rather than adsorption and desorption processes. This unilateral focus is unsurprising as the MD free energy calculations are very revealing for chemical transformations but not quite suitable for desorption during which adsorbate and adsorbent must separate ideally infinitely along the CV. Nevertheless, Li et al. demonstrated that the integration of the potential of mean force from DFT-based MD can be used to estimate adsorption entropy.[39] Obviously, the challenge is to sample anharmonic contributions to the free energy independent of a CV.

In contrast to aforementioned MD techniques, thermodynamic integration[40–42] (TI) can be used to calculate free energies relative to a reference system over transformation paths other than the reaction path.[43–48] The method becomes increasingly popular among ab initio practitioners with growing computational power available for calculations and with advances of the machine learning (ML) approaches. Temperature and Hamiltonian-based λ-paths have been exploited to compute the free energy of classical crystals[49,50] and to study phase transitions.[51–56] Very recently, Jinnouchi et al. proposed an effective combination of ML with TI using the ideal gas reference allowing for accurate ab initio calculations of the chemical potential of LiF dissolved in liquid water.[57] TI can be used to obtain anharmonic contributions with respect to a harmonic reference system. This idea has been put into practice for crystals by performing TI from Debye models to fully interacting systems.[58,59] ~~Its realization for adsorption processes and catalysis in general is limited by certain obstacles to be tackled~~

below. Its realization for adsorption processes and catalysis in general is limited by several obstacles. Most importantly, conventional TI techniques use Cartesian coordinates which are inherently unsuitable for systems with rotational and translational symmetries. An illustrative presentation of this problem is given in Section S1 of the Supporting Information (SI). While this difficulty can be overcome in simulations of simple systems by fixing the overall translations and rotations, the solution for the more general cases with internal rotational degrees of freedom (such as, e.g., a weakly interacting molecule adsorbed on a substrate) is less straightforward. Furthermore, Cartesian coordinates fail to represent molecular vibrational motions of large amplitudes[17,18,60] potentially causing unnecessarily large differences in energies between harmonic reference and fully interacting system in practical simulations. This latter effect may then lead to a significant efficiency reduction of TI calculations even for relatively simple molecular systems.

In this work we suggest a solution to some of the limitations of TI making it a practical tool in computational studies on adsorption processes, i.e., catalysis. Using rotationally and translationally invariant curvilinear coordinates our formalism allows to compute the anharmonic contribution to the free energy for any system that can be described with the harmonic approximation – independent of any reaction path. Our method allows for the theoretically exact calculation of a classical anharmonic correction to the harmonic – quantum or classical – approximation. In particular, all anharmonic quantum effects are neglected while the quantum effects described by the quantum harmonic oscillator model can be, if appropriate, directly taken into account. This is especially important, e.g., when adsorption at a wide range of temperatures is considered. Quantum corrections will be important at low temperatures where anharmonicity is small (and hence the error due to its classical treatment is small as well) but with increasing temperature the system will gradually shift to the classical regime for which our treatment is exact. This article is organized as follows: We will first review TI and describe how it can be used to determine the anharmonic contribution to the free energy starting from the harmonic reference system. We will then use

5

our implementation in the VASP program package to study increasingly complex problems, from diatomic molecules to the adsorption of small adsorbates in zeolites, which has been thoroughly investigated experimentally[61] as well as computationally[13–17,19,62–71] since the 1970s.

2 Methods

In this section, we first briefly review the thermodynamic integration (TI) technique (Section 2.1), which we adapt for the use with internal coordinates (Section 2.1.1). Our strategy for the selection of internal coordinates is discussed in Section 2.1.3. Note that a canonical (NVT) ensemble is assumed throughout this work although a generalization to other ensembles is also possible. A complementary Table of abbreviations and symbols is contained in the Supporting Information (SI).

2.1 Thermodynamic integration with a harmonic reference system

In the thermodynamic integration (TI) technique,[40–42] the free energy of a system 1 is expressed as that of the reference system 0 as follows:

$$A_1 = A_0 + \Delta A_{0 \to 1} \tag{1}$$

where $\Delta A_{0 \to 1}$ designates the Helmholtz free energy difference between 1 and 0. Depending on the properties of the investigated system, a variety of reference systems is used in literature.[50,58,59,72–75] Motivated by the fact that the harmonic approximation is commonly used for calculations of adsorption thermodynamics in solid sorbents[14,17,18,20,76–80] we focus on the harmonic reference system throughout this work. Classical and quantum harmonic approximation deviate significantly at low temperatures where the free energy of matter is dominated by quantum effects. For adsorption free energies however, this difference between theories converges rapidly to zero with increasing temperature (see SI, Section S2). For the

outlined anharmonic correction we are free to choose between the classical and quantum harmonic reference system (and their difference is negligible). Since the anharmonic correction by DFT-based MD is always classical we decided to use the classical harmonic reference system, for which the quasi-classical free energy expression writes[81]

$$A_{0,\boldsymbol{x}} = A_{\text{el}}(\boldsymbol{x}_0) - k_{\text{B}}T \sum_{i=1}^{N_{\text{vib}}} \ln \frac{k_{\text{B}}T}{\hbar\omega_i} \tag{2}$$

with the electronic free energy for the configuration corresponding to the potential energy minimum $A_{\text{el}}(\boldsymbol{x}_0)$ and the atomic position vector $\boldsymbol{x}_0$. N_{vib} is the number of vibrational degrees of freedom and ω_i is the angular frequency of vibrational mode i. Note that a harmonic dependence on Cartesian coordinates ($\boldsymbol{x}$) is assumed for the harmonic potential energy V $V_{0,\boldsymbol{x}}$ in the derivation of this equation, i.e.,

$$V(\boldsymbol{x}) = V(\boldsymbol{x}_0) + \frac{1}{2}(\boldsymbol{x} - \boldsymbol{x}_0)^T \underline{\boldsymbol{H}}^{\boldsymbol{x}}(\boldsymbol{x} - \boldsymbol{x}_0)$$

$$V_{0,\boldsymbol{x}}(\boldsymbol{x}) = V_{0,\boldsymbol{x}}(\boldsymbol{x}_0) + \frac{1}{2}(\boldsymbol{x} - \boldsymbol{x}_0)^T \underline{\boldsymbol{H}}^{\boldsymbol{x}}(\boldsymbol{x} - \boldsymbol{x}_0) \tag{3}$$

where $\underline{\boldsymbol{H}}^{\boldsymbol{x}}_{i,j} = \frac{\partial^2 V_{0,\boldsymbol{x}}(\boldsymbol{x})}{\partial x_i \partial x_j}\big|_{\boldsymbol{x}=\boldsymbol{x}_0}$ is the Hessian matrix evaluated for the structure $\boldsymbol{x}_0$ belonging to the potential energy minimum. By definition,[82] $A_{\text{el}}(\boldsymbol{x}_0) = -k_{\text{B}}T \ln \left[g \exp\left(-V_{0,\boldsymbol{x}}(\boldsymbol{x}_0)/k_{\text{B}}T \right) \right]$, where g is the electronic multiplicity. Hence, the particularly simple relation $A_{\text{el}}(\boldsymbol{x}_0) = V_{0,\boldsymbol{q}}(\boldsymbol{x}_0)$ holds when the electronic state of the system of interest is a singlet, which is the case for all systems discussed in this work. The correction term $\Delta A_{0\to1} \equiv \Delta A_{0,\boldsymbol{x}\to1}$ can be computed using thermodynamic integration TI:[40–42]

$$\Delta A_{0\to1} = \int_0^1 d\lambda \langle \mathcal{H}_1 - \mathcal{H}_0 \rangle_\lambda$$

$$\Delta A_{0,\boldsymbol{x}\to 1} = \int_0^1 d\lambda \langle \mathcal{H}_1 - \mathcal{H}_{0,\boldsymbol{x}} \rangle_\lambda \tag{4}$$

where λ is the coupling strength between the ~~systems 0 and 1~~ true physical system 1 whose potential energy V_1 is computed at the ab initio level and the harmonic reference system 0 with its potential energy defined in eq. 3., and $\langle \ldots \rangle_\lambda$ represents the NVT ensemble average of the system driven by the classical Hamiltonian

~~$$\mathcal{H}_\lambda = \lambda \mathcal{H}_1 + (1-\lambda)\mathcal{H}_0.$$~~

$$\mathcal{H}_\lambda = \lambda \mathcal{H}_1 + (1-\lambda)\mathcal{H}_{0,\boldsymbol{x}}. \tag{5}$$

Since the Hamiltonians $\mathcal{H}_{0,\boldsymbol{x}}$ and $\mathcal{H}_1$ differ only in their respective potential energy contributions $V_{0,\boldsymbol{x}}$ and V_1, eq. (4) can be cast into the form:

~~$$\Delta A_{0\to 1} = \int_0^1 d\lambda \langle V_1 - V_0 \rangle_\lambda.$$~~

$$\Delta A_{0,\boldsymbol{x}\to 1} = \int_0^1 d\lambda \langle V_1 - V_{0,\boldsymbol{x}} \rangle_\lambda. \tag{6}$$

In practice, the ensemble averages are computed using MD (in this work) or MC simulations. Typically, it is observed that the phase space volume effectively spanned by the system at the given conditions increases as λ is increased. This increase is a consequence of the transformation from harmonic to anharmonic vibrations or even to non-vibrational degrees of freedom such as internal rotations or hindered translations (e.g., when adsorbates start to diffuse through the substrate). For this reason, the integrand of eq. (4) often tends to increase in absolute value as λ reaches its upper limit, which has to be taken into account

when choosing the mesh of integration points for the evaluation of $\Delta A_{0,\boldsymbol{x}\to1}$.

2.1.1 TI in internal coordinates

One practical problem for the use of TI in chemistry is related to the fact that the commonly used Cartesian coordinates $\boldsymbol{x}$ are not insensitive to the overall rotations and translations (or any other symmetry operation) that must leave the total energy invariant. Hence, the Cartesian coordinates are intrinsically unsuitable for the use in TI simulations of gas phase molecules and weakly bound adsorption complexes.

Here we propose to overcome this problem by replacing the Cartesian coordinates by rotationally and translationally invariant internal coordinates $\boldsymbol{q} = \boldsymbol{q}(\boldsymbol{x})$, such as bond lengths, angles, torsions, and their more complex combinations, e.g., weighted sums of coordination number functions (eq. (20)). Since the force field which is harmonic in $\boldsymbol{x}$ is not necessarily equivalently harmonic in $\boldsymbol{q}$ (and *vice versa*), we express eq. (1) in the following form:

$$A_1 = A_{0,\boldsymbol{x}} + \Delta A_{0,\boldsymbol{x}\to0,\boldsymbol{q}} + \Delta A_{0,\boldsymbol{q}\to1} \tag{7}$$

where $\Delta A_{0,\boldsymbol{x}\to0,\boldsymbol{q}}$ corresponds to the transformation from the system harmonic in $\boldsymbol{x}$ to the system harmonic in $\boldsymbol{q}$, while $\Delta A_{0,\boldsymbol{q}\to1}$ is the contribution by the transformation from the system harmonic in $\boldsymbol{q}$ to the fully interacting system 1. We employ the same notation throughout this work. In consequence of the fact that eq. (7) is a sum, the anharmonic correction by TI extends the common workflow in which energy contributions are added to the total energy of stationary points on the potential energy surface (PES), see Scheme 1. For the special case of phase volume conserving coordinates (such as inter-atomic distances) the term $\Delta A_{0,\boldsymbol{x}\to0,\boldsymbol{q}}$ is zero. In general, however, this contribution does not vanish (albeit it often is very small) and its value should be taken into account. The term $\Delta A_{0,\boldsymbol{x}\to0,\boldsymbol{q}}$ corresponds to work due to a force field to force field transformation and is computationally inexpensive. For this reason, we determine this term numerically using eq. (4) combined
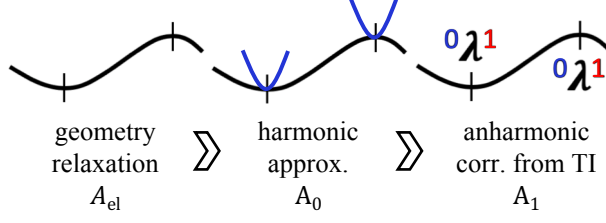
Scheme 1: Standard workflow for the computation of free energies in the harmonic approximation extended by the calculation of anharmonic contributions through thermodynamic integration (TI) as a third step.

with the Hamiltonian

$$\mathcal{H}_\lambda = \lambda \mathcal{H}_{0,\boldsymbol{q}} + (1-\lambda)\mathcal{H}_{0,\boldsymbol{x}}. \tag{8}$$

Since the kinetic energy is independent of the choice of coordinates, the Hamiltonians $\mathcal{H}_{0,\boldsymbol{x}}$ and $\mathcal{H}_{0,\boldsymbol{q}}$ for the systems harmonic in $\boldsymbol{x}$ and $\boldsymbol{q}$ differ only in their respective potential energy contributions $V(\boldsymbol{x})$ $V_{0,\boldsymbol{x}}(\boldsymbol{x})$ and $V(\boldsymbol{q})$ $V_{0,\boldsymbol{q}}(\boldsymbol{q})$ given by eqs. (3) and (9):

$$V(\boldsymbol{q}) = V(\boldsymbol{q}_0) + \frac{1}{2}(\boldsymbol{q} - \boldsymbol{q}_0)^T \underline{\boldsymbol{H}}^{\boldsymbol{q}} (\boldsymbol{q} - \boldsymbol{q}_0)$$

$$V_{0,\boldsymbol{q}}(\boldsymbol{q}) = V_{0,\boldsymbol{q}}(\boldsymbol{q}_0) + \frac{1}{2}(\boldsymbol{q} - \boldsymbol{q}_0)^T \underline{\boldsymbol{H}}^{\boldsymbol{q}} (\boldsymbol{q} - \boldsymbol{q}_0) \tag{9}$$

where $\boldsymbol{q}_0$ are the internal coordinates of the potential energy minimum, and the Hessian matrix $\underline{\boldsymbol{H}}^{\boldsymbol{q}}$ is related to $\underline{\boldsymbol{H}}^{\boldsymbol{x}}$ via

$$\underline{\boldsymbol{H}}^{\boldsymbol{q}} = \underline{\boldsymbol{A}}_{\mathbf{x}_0}^T \underline{\boldsymbol{H}}^{\boldsymbol{x}} \underline{\boldsymbol{A}}_{\mathbf{x}_0} \tag{10}$$

and

$$\underline{\boldsymbol{H}}^{\boldsymbol{x}} = \underline{\boldsymbol{B}}_{\mathbf{x}_0}^T \underline{\boldsymbol{H}}^{\boldsymbol{q}} \underline{\boldsymbol{B}}_{\mathbf{x}_0} \tag{11}$$

with $\underline{\boldsymbol{A}}$ being the Moore-Penrose pseudo-inverse of the Wilson B-matrix:[60,83]

$$\underline{\boldsymbol{B}}_{i,j} = \frac{\partial q_i}{\partial x_j}. \tag{12}$$

10

We emphasize that all terms in eqs. (10) and (11) are evaluated for the stationary point $\mathbf{x} = \mathbf{x}_0$ whose structure can be described by the internal coordinates $\mathbf{q} = \mathbf{q}_0$. The forces needed in the evaluation of the equations of motion for the atoms in a TI calculation of the term $\Delta A_{0,\boldsymbol{x}\to 0,\boldsymbol{q}}$ write

$$-\frac{\partial \mathcal{H}_\lambda}{\partial \boldsymbol{x}} = -\lambda \frac{\partial \mathcal{H}_{0,\boldsymbol{q}}}{\partial \boldsymbol{x}} - (1-\lambda)\frac{\partial \mathcal{H}_{0,\boldsymbol{x}}}{\partial \boldsymbol{x}}. \tag{13}$$

Making use of the transformation relations for the forces by any potential V:[84–88]

$$-\frac{\partial V}{\partial \boldsymbol{x}} = -\underline{\boldsymbol{B}}_{\mathsf{x}}^T \left(\frac{\partial V}{\partial \boldsymbol{q}}\right) \tag{14}$$

and

$$-\frac{\partial V}{\partial \boldsymbol{q}} = -\underline{\boldsymbol{A}}_{\mathsf{x}} \left(\frac{\partial V}{\partial \boldsymbol{x}}\right), \tag{15}$$

eq. (13) can be rearranged into the form:

$$-\frac{\partial \mathcal{H}_\lambda}{\partial \boldsymbol{x}} = -\lambda \underline{\boldsymbol{B}}_{\mathsf{x}}^T \underline{\boldsymbol{H}}^{\boldsymbol{q}}(\boldsymbol{q} - \boldsymbol{q}_0) - (1-\lambda)\underline{\boldsymbol{B}}_{\tilde{\boldsymbol{x}}_0}^T \underline{\boldsymbol{H}}^{\boldsymbol{q}} \underline{\boldsymbol{B}}_{\tilde{\boldsymbol{x}}_0}(\boldsymbol{x} - \tilde{\boldsymbol{x}}_0) \tag{16}$$

with matrix $\underline{\boldsymbol{B}}_{\boldsymbol{x}}$ and vector $\boldsymbol{q}$ being evaluated for the current geometry $\boldsymbol{x}$. ~~Importantly, the position of the minimum structure expressed in Cartesian coordinates ($\tilde{\boldsymbol{x}}_0$) must be rotated so as to match the orientation of the current $\boldsymbol{x}$, which is realized iteratively by discretization of the linear relation $d\boldsymbol{x} = \underline{\boldsymbol{A}}\,d\boldsymbol{q}$.~~ Since the molecular systems might rotate during the MD simulation, it is important to match the position of the minimum with the orientation of the current position vector $\boldsymbol{x}$, otherwise incorrect forces corresponding to the harmonic model would be generated – see Section S1 in the SI for a simple illustration of this problem. In fact, the term $\underline{\boldsymbol{B}}_{\tilde{\boldsymbol{x}}_0}^T \underline{\boldsymbol{H}}^{\boldsymbol{q}} \underline{\boldsymbol{B}}_{\tilde{\boldsymbol{x}}_0}$ in eq. (11) corresponds to the Hessian matrix of the unperturbed system expressed in rotated Cartesian coordinates. Such a rotated minimum structure, which we label $\tilde{\boldsymbol{x}}_0$, is determined iteratively by discretization of the linear relation $d\boldsymbol{x} = \underline{\boldsymbol{A}}\,d\boldsymbol{q}$. In this procedure, commonly used in the context of geometry optimization in internal coordinates,[84–88] we compute the rotated coordinates $\tilde{\boldsymbol{x}}_0$ self-consistently using

11

eq. (17) with repeated evaluations of $\tilde{\boldsymbol{q}}^{i+1}$ corresponding to the trial Cartesian vector $\tilde{\boldsymbol{x}}_0^{i+1}$ as well as $\underline{\boldsymbol{A}}_{\tilde{\boldsymbol{x}}_0^{i+1}}$ corresponding to $\tilde{\boldsymbol{x}}_0^{i+1}$ and $\tilde{\boldsymbol{q}}^{i+1}$.

$$\tilde{\boldsymbol{x}}_0^{i+1} = \tilde{\boldsymbol{x}}_0^i + \underline{\boldsymbol{A}}_{\tilde{\boldsymbol{x}}_0^i}(\boldsymbol{q}_0 - \tilde{\boldsymbol{q}}^i) \tag{17}$$

Similarly, the term $\Delta A_{0,\boldsymbol{q}\to 1}$ is computed using TI (eq. (4)) employing the Hamiltonian:

$$\mathcal{H}_\lambda = \lambda \mathcal{H}_1 + (1 - \lambda)\mathcal{H}_{0,\boldsymbol{q}}. \tag{18}$$

The forces generated by the Hamiltonian in eq. (18) are used in the evaluation of the equations of motion for the atoms in the MD simulations. ~~These forces can be written as follows:~~ Employing the transformation relation from eq. (14), these forces can be written as follows:

$$-\frac{\partial \mathcal{H}_\lambda}{\partial \boldsymbol{x}} = -\lambda \frac{\partial V(\boldsymbol{x})}{\partial \boldsymbol{x}} - (1-\lambda)\underline{\boldsymbol{B}}_{\boldsymbol{x}}^T \underline{\boldsymbol{H}}^{\boldsymbol{q}}(\boldsymbol{q} - \boldsymbol{q}_0)$$

$$-\frac{\partial \mathcal{H}_\lambda}{\partial \boldsymbol{x}} = -\lambda \frac{\partial V_1(\boldsymbol{x})}{\partial \boldsymbol{x}} - (1-\lambda)\underline{\boldsymbol{B}}_{\boldsymbol{x}}^T \underline{\boldsymbol{H}}^{\boldsymbol{q}}(\boldsymbol{q} - \boldsymbol{q}_0) \tag{19}$$

where ~~$V(\boldsymbol{x})$~~ $V_1(\boldsymbol{x})$ is the electronic energy computed using DFT.

2.1.2 Choice of the harmonic reference system

The free energy of the harmonic reference system $A_{0,\boldsymbol{x}}$ can always be computed analytically for any harmonic potential. Furthermore, TI determines $\Delta A_{0,\boldsymbol{x}\to 0,\boldsymbol{q}}$ and $\Delta A_{0,\boldsymbol{q}\to 1}$ with respect to the given reference state so that the sum $A_{0,\boldsymbol{x}} + \Delta A_{0,\boldsymbol{x}\to 0,\boldsymbol{q}} + \Delta A_{0,\boldsymbol{q}\to 1}$ equals the free energy of the physical system A_1. Therefore, the harmonic reference system can be chosen arbitrarily with no consequence for A_1. This choice can be used to improve the sampling efficiency[41] or to avoid numerical problems that occur at low λ when one or more harmonic force constants of the system are too weak. Specifically, displacements along soft modes may result in small changes in $V_{0,\boldsymbol{q}}$ but possibly cause huge changes in V_1, thus worsening the

convergence of $\langle V_1 - V_{0,\boldsymbol{q}} \rangle_\lambda$, or even leading to problems in the convergence of the electronic structure calculations. In this work, we derive the harmonic reference system from the Hessian matrix computed numerically via finite differences. The eigenvalue spectrum (i.e., the force constants) is then inspected and all values lower than a certain limit (typically $1\,\text{eV}\,\text{Å}^{-2}$) are increased to that limit while preserving the original eigenvectors. Upon such a modification, the individual contributions $A_{0,\boldsymbol{x}}$, $\Delta A_{0,\boldsymbol{x} \to 0, \boldsymbol{q}}$ and $\Delta A_{0,\boldsymbol{q} \to 1}$ are re-partitioned in such a way that the resulting A_1 remains unchanged, provided all integrals over $\langle V_{0,\boldsymbol{q}} - V_{0,\boldsymbol{x}} \rangle_\lambda$ and $\langle V_1 - V_{0,\boldsymbol{q}} \rangle_\lambda$ are converged. A demonstration of this property for the HF molecule is presented in Section 3.1.1. We note on passing that anharmonicity is an intrinsic property of the physical system. Just like A_1, anharmonicity is independent of the choice of the reference system used in the TI calculation. Therefore, anharmonicity must always be referred to the harmonic free energy determined on the basis of the actual Hessian matrix of the physical system, regardless of the choice of the harmonic reference system used in the TI calculations.

2.1.3 Choice of internal coordinates

Although well converged results of the TI should be independent of the coordinates used in the simulations, the choice of coordinates still affects the sampling efficiency. Hence some care should be taken when choosing the coordinates $\boldsymbol{q}$ for the problem at hand. In this work, the following simple rules have been used to generate $\boldsymbol{q}$: (i) bond lengths, bond angles, and torsion angles are used for molecules and for special flexible sites of a substrate (such as Brønsted sites in acid zeolites, see Section 3.2), (ii) inter-atomic distances with the atoms from the first three coordination spheres are used for all other atoms of a substrate and (iii) the position and orientation of a molecule adsorbed on the substrate is described using a function representing the coordination number (CN) of an atom i of the adsorbate with

respect to an atom j from the substrate defined as follows:[89]

$$CN_i = \sum_{j}^{N_{\text{sub}}} \sum_{\mathbf{L}} \frac{1 - (r_{ij,\mathbf{L}}/R_{ij})^9}{1 - (r_{ij,\mathbf{L}}/R_{ij})^{14}} \tag{20}$$

where the summations are over all or selected substrate atoms N_{sub} contained in a single unit cell and all translations of the unit cell $\mathbf{L} = \{\pm l_1, \pm l_2, \pm l_3\}$, $r_{ij,\mathbf{L}}$ is a distance between an atom i and atom j shifted from the original unit cell ($\mathbf{L} = 0$) by a translation $l_1 \mathbf{a}_1 + l_2 \mathbf{a}_2 + l_3 \mathbf{a}_3$ along lattice vectors $\mathbf{a}_i$, and $R_{i,j}$ is a reference distance between the atoms i and j. Since the function $\frac{1-(r_{ij,\mathbf{L}}/R_{ij})^9}{1-(r_{ij,\mathbf{L}}/R_{ij}^{14})}$ decays rapidly with increasing $r_{ij,\mathbf{L}}$, the (infinite) lattice sum in eq. (20) can be truncated when $r_{ij,\mathbf{L}}$ exceeds a certain cutoff radius (here 30 Å). Note that the local symmetry can be imposed by replacing individual primitive coordinates by their suitably chosen linear combinations. As is a common practice in atomic relaxation using internal coordinates,[90–96] the coordinate selection in point (i) is done automatically in three steps: First, distances between all pairs of atoms are computed, out of which those being shorter than a certain cutoff radius (usually based on the sum of scaled covalent radii) are used to define bond lengths. Second, all bond lengths sharing one common atom are used to define bond angles. In order to avoid numerical instability due to a singularity in the derivative of angles close to 180°, all straight angles (>165°) are excluded. Third, bond lengths and angles sharing one common atom are used to define dihedral angles. A similar scheme is also used for point (ii) but bond angles and dihedrals are replaced by distances linking the two terminal atoms. This strategy is used in order to avoid the above-mentioned numerical problems with singularities in the derivatives of angles approaching 180° during the MD. An illustration of our coordinate choice in the acidic aluminum-substituted zeolite with the chabazite topology (H-CHA) is provided in Figure 1. We note that some modifications of this strategy might be needed for different adsorption problems. In the future work, we plan to explore the use of a potentially more universal set of coordinates based on the smooth overlap of atomic positions[97] (SOAP) or components of Ewald sum (Coulomb) matrices,[98]
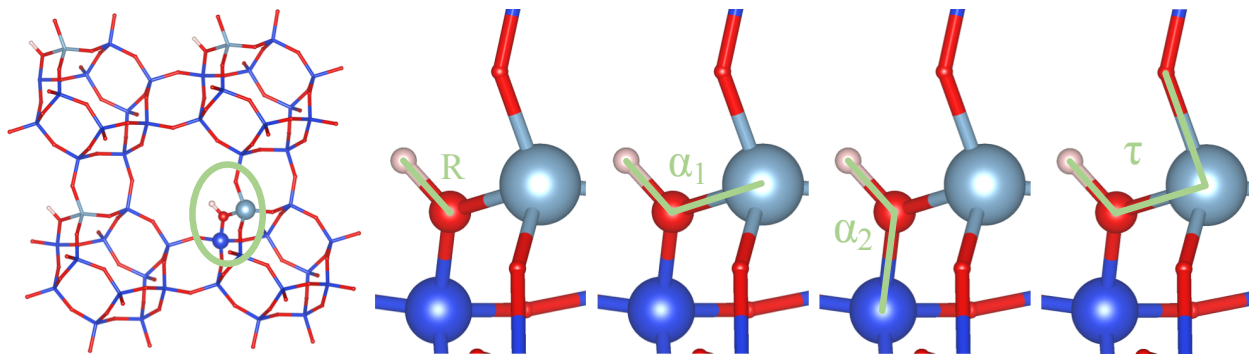
Figure 1: Definition of internal coordinates at the acidic center in H-CHA without adsorbate. The other atoms of the substrate are defined by inter-atomic distances to the atoms of their first three coordination spheres. Color code: Si: dark blue, Al: light blue, O: red, H: white.

which are successfully employed in machine learning applications in chemistry. [99]

2.2 Simulation details

Periodic density functional theory (DFT) calculations have been performed using the VASP code.[100–103] The Kohn-Sham equations have been solved variationally in a plane-wave basis set using the PAW method of Blöchl, as adapted by Kresse and Joubert with standard PAW potentials.[104,105] The PBE[106] density functional with the D2 dispersion correction (zero damping) of Grimme[107] (PBE-D2) as implemented in VASP[108] was applied for geometry optimizations and ~~molecular dynamics (MD)~~ MD simulations using an energy cutoff of $400\,\text{eV}$ for all computations but the third case study with the default value of $266.408\,\text{eV}$ for argon. Convergence criteria of $10^{-7}\,\text{eV}$ and $0.005\,\text{eV}\,\text{Å}^{-1}$ were applied to SCF-cycles and geometry optimizations, respectively. Constrained geometry relaxations have been performed using the program GADGET.[87,88] The Brillouin-zone sampling was restricted to the Γ-point.[109] Full Hessian matrices were computed for all systems using a centered finite differences scheme. DFT-based ~~molecular dynamics (MD)~~ MD simulations in the NVT ensemble were performed using the Andersen thermostat.[110] Similar to previous studies,[13] hydrogen atoms were treated as tritium (mass = $3\,\text{u}$) because this allows to use larger time steps. Consistently, the mass of tritium was also used for the computation of harmonic frequencies. Equilibration

15

periods in MD were determined with the Mann-Kendall test for trend and variation.[111] The individual specific settings, e.g., the length of MD trajectories or the integration step size, are discussed for each test case separately. The numerical integration of eq. (4) has been performed using the Simpson integration scheme adapted to irregularly spaced grid points.[112–114] The statistical error has been determined as described in section S3.2 of the ~~Supporting Information (SI)~~ SI.[115]

3 Results and discussion

3.1 Simple model systems

In order to demonstrate the validity of our approach, we start our discussion by considering three simple model systems representing one dimensional (1D) or quasi-1D problems for which exact semi-analytical solutions for ~~$\Delta A_{0\rightarrow 1}$~~ $\Delta A_{0,\boldsymbol{q}\rightarrow 1}$ can be derived from their 1D potential energy profiles. Furthermore, the three cases discussed here also illustrate the qualitative differences and importance of anharmonic effects for the free energy contribution of vibrations (HF molecule), hindered translations (argon dimer), and hindered rotations (ethane).

3.1.1 HF molecule

Due to its strongly anharmonic ($\omega_e\chi_e = 89.9\,\mathrm{cm}^{-1}$)[116] bond, the HF molecule represents a prototype system to study the anharmonicity effect on the free energy of vibration. As this effect is relatively small, a high temperature ($T = 2000\,\mathrm{K}$) was chosen in order to observe a significant deviation from the harmonic model. With the inter-atomic distance R being the only variable of the corresponding potential energy, this system represents a truly 1D problem. Since R is a phase volume conserving coordinate, the term $\Delta A_{0,\boldsymbol{x}\rightarrow 0,\boldsymbol{q}}$ is zero in this case, i.e., $A_{0,\boldsymbol{x}} = A_{0,\boldsymbol{q}}$. The anharmonic potential energy profile (~~$V_{\mathrm{full}}(R)$~~ $V_1(R)$) in Figure 2 was computed using DFT on a regular mesh of points

16

defined on the interval between $R_{\text{min}} = 0.70\,\text{Å}$ and $R_{\text{max}} = 1.40\,\text{Å}$ with grid points separated by an increment $\Delta R = 0.01\,\text{Å}$. The harmonic potential energy takes the form
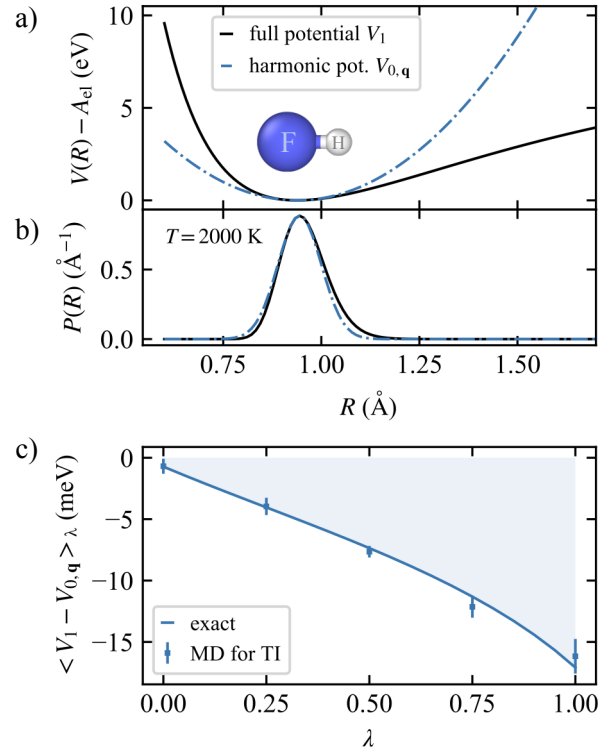
Figure 2: Case study 1 on anharmonic vibration of a covalent bond in the HF molecule. (a) Potential of the interacting system (DFT) compared to its harmonic approximation. (b) Semi-analytic probability densities emerging from the potentials. (c) TI: Comparison of the exact semi-analytic solution to the result obtained by MD runs at $2000\,\text{K}$. Integration leads to the anharmonic correction $\Delta A_{0\rightarrow1}$ $\Delta A_{0,\boldsymbol{q}\rightarrow1}$ listed in Table 1.

$V_{\text{harm}}(R) = V_{\text{harm,0}} + \frac{1}{2}C(R-R_0)^2$ $V_{0,\boldsymbol{q}}(R) = \frac{1}{2}C(R-R_0)^2 + W$ whereby the equilibrium bond length $R_0 = 0.938\,\text{Å}$ was determined using structural relaxation, the force constant $C = 56.157\,\text{eV}\,\text{Å}^{-2}$ was identified using finite differences and the constant W is irrelevant for our further discussion. With these prerequisites the exact value of $\Delta A_{0\rightarrow1}^{\text{ref}}$ $\Delta A_{0,\boldsymbol{q}\rightarrow1}^{\text{ref}}$ can be determined as follows:

$$\Delta A_{0\rightarrow1}^{\text{ref}} = -\frac{1}{\beta}\ln\left\{\frac{\int_{R_{\text{min}}}^{R_{\text{max}}} dR\, R^2 e^{-\beta\lambda V_{\text{full}}(R)}}{\int_{R_{\text{min}}}^{R_{\text{max}}} dR\, R^2 e^{-\beta\lambda V_{\text{harm}}(R)}}\right\}$$

$$\Delta A_{0,\boldsymbol{q}\to1}^{\mathrm{ref}} = -\frac{1}{\beta}\ln\left\{\frac{\int_{R_{\min}}^{R_{\max}} dR\, R^2 e^{-\beta V_1(R)}}{\int_{R_{\min}}^{R_{\max}} dR\, R^2 e^{-\beta V_{0,\boldsymbol{q}}(R)}}\right\}. \tag{21}$$

Note that the integration limits of eq. (21) were chosen so as to fully cover all values generated in the MD simulation. Indeed, the contribution of values outside the interval $R_{\min} \leq R \leq R_{\max}$ to $\Delta A_{0,\boldsymbol{q}\to1}^{\mathrm{ref}}$ is negligible at our target temperature (see Figure 2(b)). Furthermore, it follows from eq. (21) that the exact reference value of $\langle V_1 - V_{0,\boldsymbol{q}}\rangle_\lambda$ can be obtained from $V_1(R)$ and $V_{0,\boldsymbol{q}}(R)$ as follows:

$$\langle V_1 - V_{0,\boldsymbol{q}}\rangle_\lambda^{\mathrm{ref}} = \frac{\int_{R_{\min}}^{R_{\max}} dR\, R^2\, [V_1(R) - V_{0,\boldsymbol{q}}(R)]\, e^{-\beta[\lambda V_1(R)+(1-\lambda)V_{0,\boldsymbol{q}}(R)]}}{\int_{R_{\min}}^{R_{\max}} dR\, R^2\, e^{-\beta[\lambda V_1(R)+(1-\lambda)V_{0,\boldsymbol{q}}(R)]}}. \tag{22}$$

We have exploited the latter expression to evaluate the accuracy of $\langle V_1 - V_{0,\boldsymbol{q}}\rangle_\lambda$ determined from MD in Figure 2(c). The energy differences needed for the TI (eq. (4)) were obtained for five evenly spaced values of λ by MD simulations with the integration step of $0.25\,\mathrm{fs}$ and the lengths of production runs of at least $2.5\,\mathrm{ps}$ with an Andersen thermostat probability of 0.05. In all simulations, a cubic unit cell with an edge length of $15\,\text{Å}$ containing one molecule was used. As evident from Figure 2(c), the MD results for $\langle V_1 - V_{0,\boldsymbol{q}}\rangle_\lambda$ are close to the semi-analytic solution of eq. (22). Using eq. (6), we find the anharmonic correction to the vibrational free energy: $\Delta A_{0,\boldsymbol{q}\to1} = (-8.1 \pm 0.5)\,\mathrm{meV}$ which is, within the statistical error, identical to the reference value $\Delta A_{0,\boldsymbol{q}\to1}^{\mathrm{ref}} = -7.6\,\mathrm{meV}$. Moreover, this number is in excellent agreement with fully quantum mechanical treatment, as shown in Section S2.2.1 of the SI. Combined with the harmonic free energy $A_{0,\boldsymbol{x}} - A_{el}(\boldsymbol{x}_0) = 95.9\,\mathrm{meV}$, our calculations yield the total free energy of $A_1 - A_{el}(\boldsymbol{x}_0) = 87.8\,\mathrm{meV}$, while the reference value is $88.3\,\mathrm{meV}$ (see also Table 1).

Harmonic approximation $A_{0,\boldsymbol{x}}$ and anharmonic correction $\Delta A_{0\to1} = \Delta A_{0,\boldsymbol{x}\to0,\boldsymbol{q}}+$

Table 1: Results of case studies 1-3. The classical harmonic contribution (~~A_0~~$A_{0,x} - A_{el}$) was calculated using eq. (2). The anharmonic corrections ($\Delta A_{0,q\to1}$) determined by TI based on MD are compared to the semi-analytic solutions calculated using eq. (21) for case studies 1 and 2, and eq. (26) for case study 3.

Case study	T (K)	~~A_0~~$A_{0,x} - A_{el}(\boldsymbol{x}_0)$ (meV)	~~$\Delta A_{0\to1}$~~$\Delta A_{0,q\to1}$ (meV)	
			TI of MD	reference
HF molecule[a]	2000	95.9	-8.1 ± 0.5	-7.6
argon dimer[a]	300	-39.2	-28.2 ± 2.5	-27.4
ethane[b]	400	762.9	~~-41.2~~ -3.3 $\pm$ 2.2	~~-42.0~~ -4.1

[a] trivially $\Delta A_{0,\boldsymbol{x}\to0,\boldsymbol{q}} = 0$, hence $A_{0,\boldsymbol{x}} = A_{0,\boldsymbol{q}}$~~$=A_0$~~. [b] ~~$A_{0,\boldsymbol{x}} \approx A_{0,\boldsymbol{q}}$~~ $\Delta A_{0,\boldsymbol{x}\to0,\boldsymbol{q}} = (0.5 \pm 0.4)\,$meV.

$\Delta A_{0,\boldsymbol{q}\to1}$ in the calculations presented above were based on the actual force constant of HF ($C = 56.157\,\text{eV}\,\text{Å}^{-2}$) determined using a centered finite differences scheme on the DFT level of theory. We are, however, not bound to this choice. ~~In fact,~~ As discussed in Section 2.1.2, the parameters of the harmonic reference force field can be set arbitrarily without affecting the resulting value of A_1, provided all integrals ~~$\langle V_1 - V_0 \rangle_\lambda$~~ over $\langle V_{0,\boldsymbol{q}} - V_{0,\boldsymbol{x}} \rangle_\lambda$ and $\langle V_1 - V_{0,\boldsymbol{q}} \rangle_\lambda$ are converged. ~~A demonstration of this property for the HF molecule can be found in section S2 of the SI where two harmonic potentials are compared.~~ We close this section by demonstrating this property. To this end, we define a new harmonic reference system with a force constant of $28.785\,\text{eV}\,\text{Å}^{-2}$ which is half of the one in the original reference system. While $A_{0,\boldsymbol{x}\to0,\boldsymbol{q}}$ remains zero, the values of $A_{0,\boldsymbol{x}} - A_{el}$ and $\Delta A_{0,\boldsymbol{q}\to1}$ computed with this new reference are $36.1\,$meV and $52.8\,$meV, respectively. Despite this dramatic change in both terms, the resulting value of $A_1 = 88.9\,$meV is virtually identical to the value obtained with the original harmonic reference system ($87.8\,$meV), as it should be.

~~The fact that the parameters of the harmonic force field can be adjusted without affecting the result is further employed throughout this study (Section 3.2) to avoid numerical problems that occur for soft modes where displacements generating only small changes in V_0 might lead to huge changes in V_1. More generally, the parameters of V_{harm} V_0 can be fine tuned towards the smallest $\langle V_1 - V_0 \rangle_\lambda$ for all values of λ. [117,118] This subject is, however, beyond the scope of this work.~~

3.1.2   Argon dimer (Ar$_2$)

In analogy to the HF molecule discussed in Section 3.1.1, the potential energy of the argon dimer (Ar$_2$) discussed in this section is a one dimensional function of the inter-atomic distance R. In contrast to HF, however, the Ar atoms of the dimer are attracted by only a weak dispersion interaction and hence the latter system collapses already at relatively low temperatures well below $300\,\mathrm{K}$ considered here. Upon the collapse, the vibrational degree of freedom is converted into hindered translations of the atoms which can not be reasonably well described by a harmonic model. We therefore consider the argon dimer as a prototype system to study the free energy change due to dissociation. This transformation of a bond into two disjoint fragments occurs frequently in adsorption problems and chemical reactions.

As in the case of HF, the term $\Delta A_{0,\boldsymbol{x}\rightarrow 0,\boldsymbol{q}}$ equals zero and our MD results are compared to analytical solutions represented by eqs. (21) and (22). If the dimer collapses, the value of $\Delta A_{0\rightarrow 1}$ $\Delta A_{0,\boldsymbol{q}\rightarrow 1}$ will strongly depend on the volume available for the atoms to move. In our calculations, we considered only the configurations where the mutual distance of two Ar atoms did not exceed $6\,\text{Å}$ (i.e., $R_{\max} = 6.00\,\text{Å}$ was used in eq. (21)). The harmonic potential $V_{\mathrm{harm}}(R)$ $V_{0,\boldsymbol{q}}(R)$ was built using $C = 0.154\,\mathrm{eV}\,\text{Å}^{-2}$ and $R_0 = 3.705\,\text{Å}$ yielding a harmonic contribution of A_0 $A_{0,\boldsymbol{x}} - A_{el}(\boldsymbol{x}_0) = -39.2\,\mathrm{meV}$ to the free energy. The anharmonic potential energy profile ($V_{\mathrm{full}}(R)$ $V_1(R)$) was evaluated using DFT on a regular mesh of grid points defined on the interval between $R_{\min} = 2.50\,\text{Å}$ and $R_{\max} = 6.00\,\text{Å}$ with grid points separated by an increment $\Delta R = 0.10\,\text{Å}$. The λ-dependent morphing of the driving potential is shown in Figure 3(a). The In excellent agreement with the quantum mechanical description in Section S2.1.2 of the SI, the classical reference value of $\Delta A_{0\rightarrow 1}^{\mathrm{ref}}$ $\Delta A_{0,\boldsymbol{q}\rightarrow 1}^{\mathrm{ref}}$ evaluated using eq. (21) is $-27.4\,\mathrm{meV}$ resulting a in total free energy of $A_1 - A_{\mathrm{el}}(\boldsymbol{x}_0) = -66.6\,\mathrm{meV}$. For this dissociation, the anharmonic correction is in the order of magnitude of the contribution from the harmonic approximation. In comparison to the analogous HF system with a purely vibrational degree of freedom (discussed in Section 3.1.1), the anharmonic contribution is, despite the significantly lower temperature, much higher for the transformation of a vibration
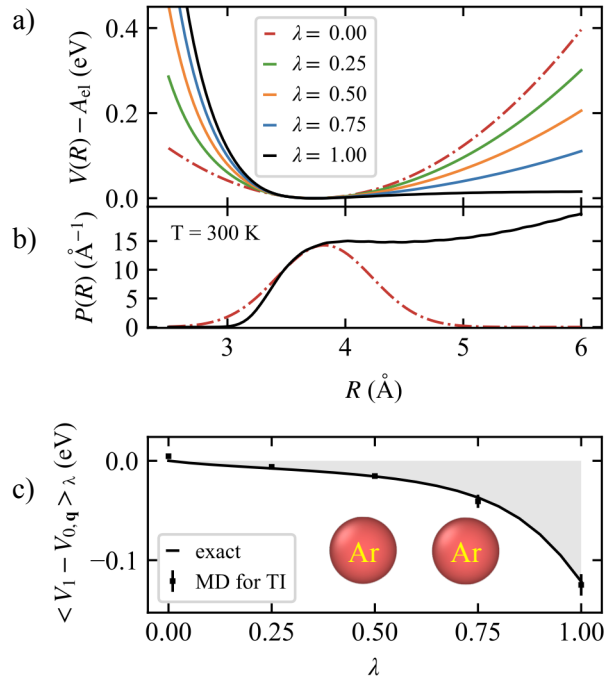
Figure 3: Case study 2 on hindered translation (dissociation) of the argon dimer. (a) Visualization of potential morphing due to the linear combination of Hamiltonians. (b) Semi-analytic probability densities for harmonic ($\lambda = 0$) and fully interacting ($\lambda = 1$) system. (c) TI: Comparison of exact semi-analytic solution to averaged energy differences obtained by MD runs at $300\,\mathrm{K}$. Integration leads to the anharmonic correction $\Delta A_{0 \to 1}\ \Delta A_{0,\boldsymbol{q} \to 1}$.

into translation.

Owing to the large atomic mass of Ar, the MD simulations have been conducted with an integration step size of $5\,\mathrm{fs}$ and an Andersen thermostat probability of 0.1. The length of the production period for each value of λ was at least $45\,\mathrm{ps}$. A cubic box with an edge size of $15\,\text{Å}$ containing one Ar_2 was used and the condition $R \leq R_{\max}$ was applied *a posteriori* by expressing the average $\langle V_1 - V_{0,q}\rangle_\lambda$ on the subset of MD frames where the condition was met as follows:

$$\langle V_1 - V_0\rangle_\lambda = \frac{\int_0^{R_{\max}} dR \int d\boldsymbol{p}\, d\boldsymbol{q}(V_1(\boldsymbol{q}) - V_0(\boldsymbol{q}))\delta(R - R(\boldsymbol{q}))e^{-\mathcal{H}_\lambda(\boldsymbol{p},\boldsymbol{q})/k_\mathrm{B}T}}{\int_0^{R_{\max}} dR \int d\boldsymbol{p}\, d\boldsymbol{q}\,\delta(R - R(\boldsymbol{q}))e^{-\mathcal{H}_\lambda(\boldsymbol{p},\boldsymbol{q})/k_\mathrm{B}T}} \tag{23}$$

$$\langle V_1 - V_{0,\boldsymbol{x}}\rangle_\lambda = \frac{\int_0^{R_{\max}} dR \int d\boldsymbol{p}\, d\boldsymbol{x}(V_1(\boldsymbol{q}) - V_{0,q}(\boldsymbol{x}))\delta(R - R(\boldsymbol{x}))e^{-\mathcal{H}_\lambda(\boldsymbol{p},\boldsymbol{x})/k_\mathrm{B}T}}{\int_0^{R_{\max}} dR \int d\boldsymbol{p}\, d\boldsymbol{x}\,\delta(R - R(\boldsymbol{x}))e^{-\mathcal{H}_\lambda(\boldsymbol{p},\boldsymbol{x})/k_\mathrm{B}T}} \tag{24}$$

with $\boldsymbol{x}$ and $\boldsymbol{p}$ being the atomic positions and momenta respectively. A visual inspection of the configurations generated for $\lambda = 1$ (corresponding to MD driven by a full DFT potential) confirmed that the argon dimer was indeed unstable and collapsed. As shown in Figure 3, the average values $\langle V_1 - V_{0,q}\rangle_\lambda$ evaluated for five evenly spaced values of λ are close to the reference results obtained from eq. (22). The value of $\Delta A_{0,q\to 1} = (-28.2 \pm 2.5)\,\mathrm{meV}$ computed from MD is therefore in excellent agreement with $\Delta A_{0,q\to 1}^{\mathrm{ref}}$ (see also Table 1).

3.1.3 Ethane molecule

Unlike the two systems discussed above, the ethane molecule possesses multiple vibrational degrees of freedom, which can be seen in the vibrational density of states (VDOS) in Figure 4. Importantly, however, it also contains one vibrational degree of freedom that can be converted into an internal rotation corresponding to a mutual rotation of two CH_3 groups upon a thermal excitation at a modest temperature. Since the anharmonic contribution of vibrations is by orders of magnitude smaller than that of rotations or translations, the former can

be neglected at low temperatures and the term $\cancel{\Delta A_{0\to1}^{\mathrm{ref}}}\ \Delta A_{0,\boldsymbol{q}\to1}^{\mathrm{ref}}$ can thus be effectively determined from a 1D potential energy depending on a suitably chosen geometric parameter driving the internal rotation. For this purpose, we choose a linear combination τ of torsional angles τ_1, τ_2 and τ_3 shown in Figure 5(c):

$$\tau = \frac{1}{3}\left(\tau_1 + \tau_2 + \tau_3\right). \tag{25}$$

Clearly, the potential $\cancel{V_{\mathrm{full}}(\tau)}\ V_1(\tau)$ is invariant with internal rotation by $120°$, thus reflecting the basic symmetry of ethane (see Figure 5). In fact, τ as defined above is nearly a perfect representation of the vibrational eigenmode corresponding to a hindered rotation of the CH_3 groups, which is evident from Figure 4 showing the ~~vibrational density of states~~ VDOS of ethane before and after imposing a constraint on the value of τ. Obviously, fixing τ leads to
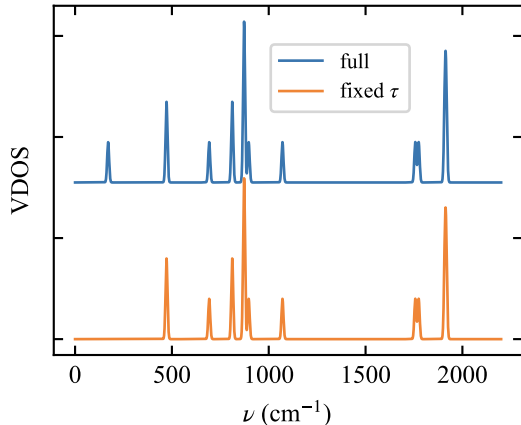
Figure 4: Vibrational density of states (VDOS) computed from the (un-)constrained Hessian matrix for ethane without (full) and with (fixed τ) a constraint imposed on the parameter τ defined by eq. (25). Consistently, the mass of tritium was used for H atoms.

a complete elimination of one vibrational mode while the remaining modes remain virtually unaffected.

The analogue of eq. (21) representing our semi-analytic reference for the anharmonic

contribution to the free energy writes:

$$\Delta A^{\mathrm{ref}}_{0\to1} = -\frac{1}{\beta}\ln\left\{\frac{\int_{-\pi}^{\pi}d\tau\, e^{-\beta\lambda V_{\mathrm{full}}(\tau)}}{\int_{-\pi}^{\pi}d\tau\, e^{-\beta\lambda V_{\mathrm{harm}}(\tau)}}\right\}$$

$$\Delta A^{\mathrm{ref}}_{0,\boldsymbol{q}\to1} = -\frac{1}{\beta}\ln\left\{\frac{\int_{-\pi}^{\pi}d\tau\, e^{-\beta V_1(\tau)}}{\int_{-\pi}^{\pi}d\tau\, e^{-\beta V_{0,\boldsymbol{q}}(\tau)}}\right\} - \frac{1}{\beta}\ln\left(\frac{1}{\sigma}\right) \tag{26}$$

where the first summand corresponds to the term $\Delta A'_{0,\boldsymbol{q}\to1}$ that is obtained by the TI approach while the latter $(-\frac{1}{\beta}\ln\left(\frac{1}{\sigma}\right))$ originates from the intrinsic permutational symmetry ($\sigma = 3$) of ethane and needs to be considered in both reference calculation and TI approach. ~~with the~~ The harmonic potential $~~V_{\mathrm{harm}}(\tau) = V_{\mathrm{harm},0} + \frac{1}{2}C(\tau-\tau_0)^2~~$ is $V_{0,\boldsymbol{q}}(\tau) = \frac{1}{2}C(\tau-\tau_0)^2 + W$ whereby the equilibrium value $\tau_0 = -1.047\,\mathrm{rad}$ was determined using structural relaxation, the force constant $C = 0.508\,\mathrm{eV\,rad}^{-2}$ was identified using finite differences at the DFT level of theory and the constant W is irrelevant for our further discussion. The anharmonic potential ($~~V_{\mathrm{full}}(\tau)~~$ $V_1(\tau)$) has been evaluated using DFT on a grid defined in the range $-\pi \le \tau \le \pi$, with grid points separated by $\sim 0.15\,\mathrm{rad}$. Specifically, the value of $~~V_{\mathrm{full}}~~$ V_1 for each grid point was determined by means of constrained relaxations with fixed τ. It can be seen in Figure 5(a) how the potential morphs with shifting values of λ so that rotations become energetically feasible. Furthermore, Figure 5(b) shows the probability density as a function of the torsion angle from which it is clear that only one out of three minima is sampled in MD driven by the harmonic potential. Moreover, it becomes clear that the discontinuity of the driving potential that emerges for $\lambda < 1$ is visited with a very low likelihood during our simulations and hence it does not pose a practical problem in our simulations. The harmonic contribution to the free energy determined at $400\,\mathrm{K}$ is $~~A_0~~ A_{0,\boldsymbol{x}} - A_{\mathrm{el}}(\boldsymbol{x}_0) = 762.9\,\mathrm{meV}$. ~~The free energy $\Delta A_{0,\boldsymbol{x}\to0,\boldsymbol{q}}$ corresponding to the force field to force field transformation was computed as described in Section 2.1.1.~~ The free energy $\Delta A_{0,\boldsymbol{x}\to0,\boldsymbol{q}}$ representing the free energy difference between the system harmonic in internal coordinates (i.e., driven by the Hessian matrix $\underline{\boldsymbol{H}}^{\boldsymbol{q}}$) and the system harmonic in
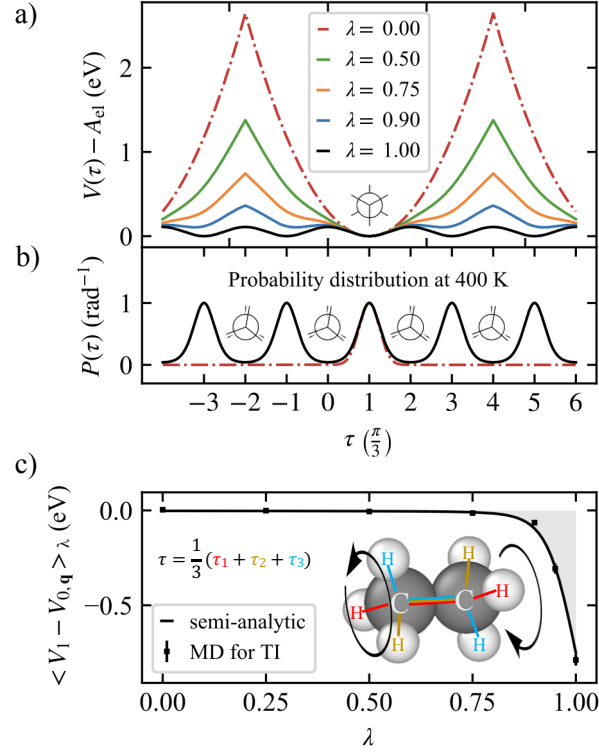
Figure 5: Case study 3 on the hindered internal rotation of ethane. (a) Visualization of potential morphing due to the linear combination of Hamiltonians. (b) Semi-analytic probability densities for harmonic ($\lambda = 0$) and fully interacting ($\lambda = 1$) system. (c) TI: Comparison of semi-analytic solution (solid line) to averaged energy differences obtained by MD runs for seven values of λ at $400\,\mathrm{K}$. Integration leads to $\Delta A'_{0,\boldsymbol{q}\to 1}$ from which the anharmonic correction $\Delta A_{0\to 1}$ $\Delta A_{0,\boldsymbol{q}\to 1}$ is obtained under consideration of the permutational symmetry.

Cartesian coordinates (i.e., driven by the Hessian matrix $\underline{\boldsymbol{H}}^{\boldsymbol{x}}$) was computed as described in Section 2.1.1. For this purpose, MD simulations for five different regularly spaced values of λ have been performed with an integration step of $0.5\,\mathrm{fs}$. The length of each simulation was $50\,\mathrm{ps}$ and an Andersen thermostat probability of 0.05 was used. The Hessian matrix $\underline{\boldsymbol{H}}^{\boldsymbol{x}}$ has been computed for the relaxed geometry. The internal coordinates $\boldsymbol{q}$ used to define the harmonic force field consisted of the geometric parameter τ from eq. (25), and the set of inter-atomic distances and angles generated as described in Section 2.1.3. The computed value of $\Delta A_{0,\boldsymbol{x}\to 0,\boldsymbol{q}} = (0.5 \pm 0.4)\,\mathrm{meV}$ is ~~almost negligible~~ not zero in contrast to the case studies with truly 1D potentials. Combined with $\Delta A_{0,\boldsymbol{q}\to 1}^{\mathrm{ref}} = ~~-42.0\,\mathrm{meV}~~ -4.1\,\mathrm{meV}$ (Table 1), the total ionic free energy $A_1 - A_{\mathrm{el}}(\boldsymbol{x}_0)$ is ~~805.4 meV~~ 760.1 meV. Again, our classical reference value is in excellent agreement with quantum mechanical treatment as shown in Section S2.1.3 of the SI. Hence, ~~as expected,~~ in our study the anharmonic contribution of a hindered rotation is ~~comparable to that of a hindered translation (see Section 3.1.2), which are both orders of magnitude greater than that of single vibration (see Section 3.1.1)~~ noticeable already at modest temperature but one order of magnitude smaller than that of a hindered translation.

~~DFT-based MD simulations were performed to determine the term $\Delta A_{0,\boldsymbol{q}\to 1}$ for seven different values of λ.~~ DFT-based MD simulations were performed to determine $\Delta A_{0,\boldsymbol{q}\to 1}$ representing the free energy difference between the fully interacting system (as described by DFT) and the system harmonic in internal coordinates, using an integration mesh with seven different values of λ. In addition to the five points of the regular grid used in the $\Delta A_{0,\boldsymbol{x}\to 0,\boldsymbol{q}}$ calculations, two extra points ($\lambda = 0.90$ and 0.95) were added to improve the sampling in the region with rapidly changing ~~$\langle V_1 - V_0\rangle_\lambda$~~ $\langle V_1 - V_{0,\boldsymbol{q}}\rangle_\lambda$ (see Figure 5). The equations of motion were integrated with a step size of $0.5\,\mathrm{fs}$. Due to the slow and infrequent internal rotations of CH_3 occurring when the harmonic potential is replaced by the full potential, the convergence of ~~$\langle V_1 - V_0\rangle_\lambda$~~ $\langle V_1 - V_{0,\boldsymbol{q}}\rangle_\lambda$ slowed down with increasing λ. We therefore used production periods of variable length which ranged between $15\,\mathrm{ps}$ ($\lambda = 0.0$) to $150\,\mathrm{ps}$ ($\lambda = 1.0$). A cubic box with an edge size of $15\,\mathrm{Å}$ containing one molecule was

used in the simulations. As shown in Figure 5(c), the ~~$\langle V_1 - V_0 \rangle_\lambda$~~ $\langle V_1 - V_{0,\boldsymbol{q}} \rangle_\lambda$ computed from MD agree well with the reference data. The computed ~~$\Delta A_{0\to1}$ $((-41.2 \pm 2.2)\,\mathrm{meV})$~~ $\Delta A'_{0,\boldsymbol{q}\to1} = (-41.2 \pm 2.2)\,\mathrm{meV}$ is therefore in excellent agreement with ~~$\Delta A^{\mathrm{ref}}_{0\to1}$~~ the first term $(-42.0\,\mathrm{meV})$ of the reference eq. (26). Under consideration of the permutational symmetry (second term in eq. (26)) we obtain $\Delta A_{0,\boldsymbol{q}\to1} = \Delta A'_{0,\boldsymbol{q}\to1} - \frac{1}{\beta}\ln\left(\frac{1}{\sigma}\right) = (-3.3 \pm 2.2)\,\mathrm{meV}$ (see also Table 1).

3.1.4 Summary of the case studies

The simple models discussed in this section can be considered a test for the correctness of our implementation of TI with internal coordinates. To this end, we compared our numerical data with the reference semi-analytical results and excellent agreement has been achieved. Furthermore, the three case studies showed that different types of degrees of freedom contribute to anharmonicity differently. From the study on the HF molecule it can be learned that the anharmonic contribution of vibration in covalently bound systems is very small at ambient temperatures and it can be neglected in most cases. Our results for the argon dimer ~~and ethane~~ show that the harmonic approximation fails in the description of hindered translations ~~and rotations~~ (dissociation) and this failure is both qualitative and quantitative. For this reason the anharmonic correction to the free energy is large in ~~these cases~~ this case. The hindered internal rotation of ethane contributes noticeable anharmonicity already at $400\,\mathrm{K}$ which is by one order of magnitude smaller than that of the hindered translation. Standard errors of the TI are well below $5\,\mathrm{meV}$. For the following adsorption study we keep in mind that the ~~harmonic Hessian matrix~~ harmonic reference system can be chosen arbitrarily (see Section 2.1.2).

3.2 Adsorption of Ar and N_2 in acid chabazite

The relevance of anharmonicity for adsorption processes in heterogeneous catalysis is often ignored or at best estimated by the more or less coarse techniques mentioned in the intro-

duction. Our presented TI approach can be used to calculate anharmonic corrections for adsorption processes on the DFT level of theory using MD. Here, we apply the concept to study two adsorbates (N_2, Ar) in the chabazite zeolite at $200\,\mathrm{K}$. As we discuss below, these two systems exhibit qualitatively different behavior with respect to the stability of the complexes formed upon adsorption. The Gibbs free energies of adsorption ($\Delta_{\mathrm{ads}}G$) at $200\,\mathrm{K}$ deduced from the data reported in the experimental work of Barrer and Davies[61] (see Section S4 in the SI) are $-24\,\mathrm{meV}$ and $-45\,\mathrm{meV}$ for Ar and N_2, respectively. ~~The~~ According to our calculations, the harmonic approximation evaluated at the PBE-D2 level tends to overestimate these values with $+26\,\mathrm{meV}$ and $-24\,\mathrm{meV}$ for Ar and N_2, respectively. As shown in our analysis of the model system Ar_2 (see Section 3.1.2), the harmonic approximation restricts the motion of atoms that are not bound by chemical bonds leading to a significant overestimation of the free energy. Similarly, the harmonic approximation restricts the adsorbate@substrate systems to configurations corresponding to the adsorption complexes in which the adsorbate is attached to the proton of the Brønsted acid site (see insets in Figure 6). Just as in the model Ar_2 case, the shift from harmonic $(V_{0,\boldsymbol{x}})$ to full DFT (V_1) interaction causes significant changes in the behavior of the adsorbate. These qualitative changes can be best seen from radial distribution functions (RDF) computed using MD for the $H-Ar$ and $H-N$ pairs (see Figure 6). The peak of the RDF for Ar adsorption in Figure 6(a) computed using the potential harmonic in Cartesian coordinates $\boldsymbol{x}$ (blue line) is relatively narrow, approximately Gaussian-shaped, and centered at the distance found in the relaxed structure ($2.4\,\text{Å}$). The same peak computed from MD driven by the fully anharmonic potential (green line) is broadened, its maximum becomes less pronounced and is shifted towards longer inter-atomic separation ($2.7\,\text{Å}$). This broadening of the RDF and the non-vanishing probability at long range clearly signify a higher entropy of the system driven by the anharmonic model compared to its harmonic counterpart. The specific interaction between N_2 and the Brønsted site of the zeolite is more significant than in the case of Ar adsorption ($164.0\,\mathrm{meV}$ vs. $36.8\,\mathrm{meV}$) *JA: where do these two numbers come from?* and the
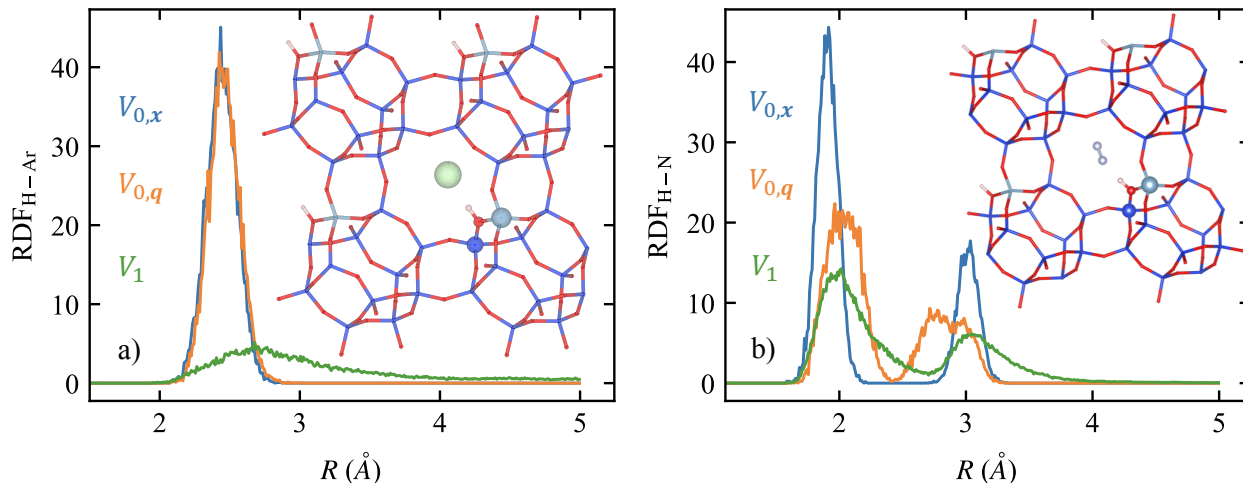
Figure 6: Partial radial distribution functions (RDF) versus inter-atomic distance (R) computed for the pairs of proton and adsorbate atoms for (a) Ar in H-CHA and (b) N_2 in H-CHA. ~~Results obtained using MD driven by harmonic and fully anharmonic potential are presented.~~ The results were obtained from MD driven by the full PBE-D2 (V_1) potential, by the potential harmonic in Cartesian coordinates ($V_{0,\boldsymbol{x}}$), and by the potential harmonic in internal coordinates ($V_{0,\boldsymbol{q}}$). The depicted zeolite structure (color code similar to Figure 1) was described by distance coordinates only except for the central adsorbate atoms (Ar, i.e., N_2) and the framework atoms at the acidic center highlighted as spheres.

adsorption complex in Figure 6(b) similar to the potential energy minimum indeed exists with a greater likelihood at our target temperature. Nevertheless, the complex is not stable all the time – rather it collapses and is recreated frequently during the MD. The shift from the potential harmonic in Cartesian coordinates to the potential harmonic in internal coordinates and eventually to the full interaction potential is accompanied by a broadening of the RDF peaks (Figure 6(b)) and a change in their shape from relatively narrow Gaussians to broader asymmetric bands. Furthermore, in consequence of temporal collapses of the adsorption complex and in contrast to the harmonic model, the RDF has non-vanishing values in the region between the two maxima. Despite the distinctions, the structure of the RDF and the positions of its maxima remain similar.

In our MD calculations, the three systems, namely the clean substrate, the adsorbate in the substrate and the free adsorbate in gas phase were treated separately. ~~All simulations were performed with the primitive unit cell of chabazite in Figure S6 of the SI.~~ A consistent

The ratio of Al/Si = 1/11 has been used in the structural model of chabazite and the proton occupied position O(1),[119] which belongs to most populated H sittings in this zeolite.[120] All TI MD calculations have been performed for seven different values of λ (0.00, 0.25, 0.50, 0.75, 0.90, 0.95, 1.00) plus several additional points defined if the $\langle V_1 - V_0 \rangle_\lambda$ $\langle V_1 - V_{0,\boldsymbol{q}} \rangle_\lambda$ term changed rapidly with λ (*vide infra*). As we have shown in Section 3.1.1, the anharmonicity of a single bond is very small even at temperatures as high as $2000\,\mathrm{K}$. We therefore neglect this contribution to the free energy of the N_2 molecule in gas phase, i.e., the N$-$N vibration is treated fully harmonically. Furthermore, rotational degrees of freedom of free N_2 are treated using the rigid rotor approximation.[5] The translational degrees of freedom of free adsorbate particles were treated using the ideal gas approximation,[5] whereby a reference pressure of $101\,325\,\mathrm{kPa}$ has been considered. The computed total free energies (including total electronic energies) of the adsorbate particles are $-0.286\,\mathrm{eV}$ (Ar) and $-16.873\,\mathrm{eV}$ (N_2). The Gibbs free energy of adsorption is computed as

$$\Delta_{\mathrm{ads}}G = A_{1,\mathrm{A@S}} - A_{1,\mathrm{S}} - G_{0,\mathrm{A}} \tag{27}$$

with the anharmonic Helmholtz free energies of the adsorbate in the substrate ($A_{1,\mathrm{A@S}}$) and the clean substrate ($A_{1,\mathrm{S}}$) as well as the Gibbs free energy of the gas phase adsorbate ($G_{0,\mathrm{A}}$) determined using the harmonic oscillator, rigid rotor, and ideal gas approximations. We note that the cancellation of the pV terms for the A@S and S systems is a reasonable assumption in eq. (27) since the substrate is a crystalline material and the concentration of adsorbate in the A@S system is relatively low – hence volume changes of the substrate due to adsorption should be small.

For our TI calculations the internal coordinates of the clean substrate were chosen as described in Section 2.1.3, whereby the proton position was described by four special internal coordinates: the OH bond length, the bond angles $H-O-Al$ and $H-O-Si$, and the initially smallest torsion $H-O-Al-O$ (the atoms involved in definitions of these coordinates are shown in Figure 1). In order to avoid numerical problems in simulations with $\lambda = 0$, all eigenvalues of the Hessian matrix have been increased to $1\,\mathrm{eV\,\mathring{A}}^{-2}$ if they were lower than this limit (see Section 2.1.2). The harmonic free energy contribution $A_{0,x}$ computed using the modified Hessian matrix ($\underline{\boldsymbol{H}}^x$) is $-286.968\,\mathrm{eV}$, which is to be compared to $-287.077\,\mathrm{eV}$ determined for the unmodified $\underline{\boldsymbol{H}}^x$. The length of all MD simulations was $500\,\mathrm{ps}$. The integration step used in the inexpensive force field to force field calculations was $0.5\,\mathrm{fs}$ while a larger step of $1\,\mathrm{fs}$ was used in the DFT calculations. As expected, the computed value of $\Delta A_{0,x\to0,q}$ is very small ((-5 ± 0)\,meV), which can be attributed to the low temperature (indeed, $\Delta A_{0,x\to0,q}$ tends to zero with decreasing temperature) and the limited structural variation allowed by the framework structure with all atoms being connected by strong covalent bonds. The term $\Delta A_{0,q\to1}$, on the other hand, takes a significantly greater value of (-99 ± 0)\,meV. Plugging all free energy contributions into eq. (7), the computed free energy of the substrate is $A_1 = -287.072\,\mathrm{eV}$. Comparing this value with the harmonic free energy determined using the original unmodified $\underline{\boldsymbol{H}}^x$ ($-287.077\,\mathrm{eV}$) we recognize that the anharmonicity of the substrate at our target temperature is essentially negligible.

For the interacting system of Ar and chabazite, the set of internal coordinates used for the clean substrate (*vide supra*) was extended by the CN coordinate (eq. (20)) defined for all $Ar-Si$ and $Ar-Al$ pairs. The eigenvalues of $\underline{\boldsymbol{H}}^x$ for this system have been increased to $2\,\mathrm{eV\,\mathring{A}}^{-2}$ if they were lower than this limit (see Section 2.1.2). The harmonic free energy contribution $A_{0,x}$ computed using the modified $\underline{\boldsymbol{H}}^x$ is $-287.102\,\mathrm{eV}$, which is to be compared to $-287.337\,\mathrm{eV}$ determined for the unmodified $\underline{\boldsymbol{H}}^x$. The setting of the MD simulations for the interacting system was identical to that used for the clean substrate. An extra integration point $\lambda = 0.99$ was used in the calculation of $\Delta A_{0,q\to1}$.

As in the case of the clean zeolite, the computed value of $\Delta A_{0,\boldsymbol{x}\to0,\boldsymbol{q}}$ is very small and barely statistically significant $((-2\pm0)\,\text{meV})$, while the term ~~$\Delta A_{0\to1}$~~ $\Delta A_{0,\boldsymbol{q}\to1}$ is as large as $(-271\pm1)\,\text{meV}$. Combining the free energy contributions, eq. (7) yields $A_1 = -287.375\,\text{eV}$, which is to be compared with the harmonic free energy of $-287.337\,\text{eV}$ determined using the original unmodified $\underline{\boldsymbol{H}}^{\boldsymbol{x}}$. Hence, in line with our expectation, the anharmonicity lowers the free energy of the interacting system, which is given by the transformation of a part of the vibrations involving Ar into hindered translations, thus increasing the entropy of Ar adsorbed in the zeolite. Using eq. (27) with the free energies determined for the clean substrate, free Ar in gas-phase and the interacting system (see Table 2), we arrive at $\Delta_{\text{ads}}G = $ ~~$(-18\pm2)\,\text{meV}$~~ $(-17\pm2)\,\text{meV}$, which is ~~$44\,\text{meV}$~~ $43\,\text{meV}$ lower compared to the prediction made using the harmonic approximation (see Table 3). Remarkably, our result predicted using TI is very close to the experimental value reported by Barrer and Davies[61] (although we admit that this level of agreement is fortuitous to some extent).

The internal coordinates chosen for the interacting system of N_2 and chabazite consisted of those used for the clean substrate (*vide supra*) extended by the $N-N$ distance and the CN coordinates (eq. (20)) defined for all $N-Si$ and $N-Al$ pairs. All computed contributions to A_1 are listed in Table 2. The Hessian matrix eigenspectrum has been modified so that no force constant was lower than $2\,\text{eV}\,\text{Å}^{-2}$ (see Section 2.1.2). For this modified harmonic reference model, a harmonic free energy contribution of $-303.736\,\text{eV}$ has been determined, while the value of ~~A_0~~ $A_{0,\boldsymbol{x}}$ for the unmodified $\underline{\boldsymbol{H}}^{\boldsymbol{x}}$ is $-303.974\,\text{eV}$. Owing to a relatively large variation of the term ~~$\langle V_1 - V_0 \rangle_\lambda$~~ $\langle V_1 - V_{0,\boldsymbol{q}} \rangle_\lambda$ with λ, three extra integration points ($\lambda = 0.990$, 0.995 and 0.999) have been used in the $\Delta A_{0,\boldsymbol{x}\to0,\boldsymbol{q}}$ calculation. As evident from Figure 6(b), the coordinate transformation in the harmonic model causes significant changes in the behavior of adsorbed N_2. Consequently, the computed $\Delta A_{0,\boldsymbol{x}\to0,\boldsymbol{q}}$ of $(-22\pm1)\,\text{meV}$ represents a significant contribution to the anharmonic part of the adsorption free energy. Indeed, a transformation to a suitable set of coordinates can allow to capture a part of anharmonicity even within a harmonic model. Finally, the computed value of ~~$\Delta A_{0\to1}$~~ $\Delta A_{0,\boldsymbol{q}\to1}$ is $(-245\pm5)\,\text{meV}$

and the total free energy of the adsorbate is $(-304.003 \pm 5.000)\,\mathrm{eV}$. Comparing the latter result with the value of $-303.974\,\mathrm{eV}$ predicted by the unmodified harmonic model it is obvious that the temporary collapse of the adsorption complex observed in a fully interacting model leads to a decrease (via increased entropy) of free energy by ~~28 meV~~ 29 meV. Consequently, the Gibbs free energy of adsorption computed using TI (~~$(-59 \pm 5)\,\mathrm{meV}$~~ $(-58 \pm 5)\,\mathrm{meV}$) is lower than that obtained using the harmonic approximation. The TI value is also slightly closer to the experimental value of $-45\,\mathrm{meV}$ although the improvement with respect to the harmonic approximation is less significant than for the adsorption of Ar. Clearly, a careful choice of the density functional approximation and dispersion correction method would be needed in order to further improve the accuracy of adsorption free energy calculations.

Table 2: Contributions to the free energies A_1 in eV at $200\,\mathrm{K}$ and a reference pressure of $101\,325\,\mathrm{kPa}$. As usual, in all calculations the mass of tritium was used for H atoms.

System	$A_{0,\boldsymbol{x}}$ +	$\Delta A_{0,\boldsymbol{x}\to 0,\boldsymbol{q}}$ +	$\Delta A_{0,\boldsymbol{q}\to 1}$ =	A_1
Ar	~~-0.2857~~ -0.286[a] +	0^b +	0 =	~~-0.2857~~ -0.286
N_2	~~-16.8727~~ -16.873[c] +	0^b +	0^d =	~~-16.8727~~ -16.873
chabazite	-286.968 +	-0.005 ± 0.000 +	-0.099 ± 0.001 =	-287.072 ± 0.004
Ar@chabazite	-287.102 +	-0.002 ± 0.000 +	-0.271 ± 0.001 =	-287.375 ± 0.002
N_2@chabazite	-303.736 +	-0.022 ± 0.001 +	-0.245 ± 0.005 =	-304.003 ± 0.005

[a] ideal gas approximation. [b] $A_{0,\boldsymbol{x}} = A_{0,\boldsymbol{q}}$. [c] harmonic oscillator/ideal gas/linear rigid rotor approximations. [d] negligible.

Table 3: Comparison of simulation results to experimental values for adsorption Gibbs free energies at $200\,\mathrm{K}$ in meV. TI approach and harmonic approx. were computed on the DFT level of theory.

Adsorbate	Experiment[61]	TI approach	harmonic approx.
Ar	-24	~~-18 ± 2~~ -17 ± 2	$+26$
N_2	-45	~~-59 ± 5~~ -58 ± 5	-24

4 Summary and conclusion

We presented thermodynamic integration (TI) as a tool to compute anharmonic corrections to the free energies of molecular and periodically extended systems. Using translationally

and rotationally invariant internal (curvilinear) coordinates we overcame the significant limitation of the TI approach traditionally formulated in Cartesian coordinates. Our variant of the method was demonstrated in three case studies and then applied to study adsorption energies of N_2 and Ar in the acidic chabazite zeolite. Hindered rotations and translations (dissociation) which are poorly described by the harmonic approximation were identified to cause significant anharmonic contributions to the free energy (translation more than rotation) while the anharmonic contributions of vibrations of covalent bonds are rather negligible. In comparison with experimental data from literature we observed that the anharmonic correction improves the accuracy of predicted adsorption free energies.

In principle, other popular simulation methods, such as the Blue Moon ensemble approach[29,30] or Umbrella sampling[31–33] could be employed to determine the adsorption free energy. These methods, however, require the sampling of the configuration space over a continuous reaction coordinate, which is extremely impractical for adsorption problems. In particular, the structural model of the substrate would have to be large with a wide vacuum gap so as to allow both the simulation of the sorbate adsorbed in bulk (unperturbed by surface effects) and the simulation of the desorbed sorbate unperturbed by interactions with the substrate. Hence, the presented TI method requiring simulations of only initial and final states without the necessity to sample over the corresponding transformation path in space, is perfectly suited to study adsorption free energies or individual rate determining steps in multi-step reaction cascades and could thus become a very useful tool for computational catalysis.

Another MD based method that is used in the literature to access the free energy of molecules and extended systems is the quasi-harmonic approximation (QHA).[121] In QHA the harmonic oscillator model is used with renormalized vibrational frequencies determined from MD via Fourier transformation of the velocity autocorrelation function (VAF). Such an approach, for instance, recently used to study ethanol adsorption in H-ZSM5,[15] solves a part but not all problems associated with the harmonic approximation. The frequency renor-

malization allows to consider thermal effects related to the thermal expansion of bonds. Furthermore, the frequencies emerging from MD are anharmonic and hence their use can account for a part of the vibrational anharmonicity. Nevertheless, we note that the latter are used in connection with the expressions derived for the harmonic oscillator, which is not rigorously correct for a general anharmonic case. Even worse, the QHA method cannot account for non-vibrational aperiodic degrees of freedom like hindered translations with no or negligible contribution to the VAF. Finally, the need for accurate accounting of the time correlation imposes a serious constraint on the simulation setting. The stochastic thermostats such as Andersen[110] or Langevin[122,123] cannot be used since the stochastic collisions quickly destroy any time correlations between atomic positions. The deterministic thermostats such as Nosé-Hoover[124,125] or Nosé-Hoover chains[126] must be adjusted with great care because the contributions from fictitious degrees of freedom of the thermostat can bias the computed VDOS. The VAF is therefore often computed in the microcanonical regime, which however, imposes a limitation on the length of the trajectory because the temperature can drift away from the desired value. Also, the need for an accurate VDOS implies that a relatively small integration step must be used in a QHA calculation, which in turn leads to less efficient exploration of remote parts of the accessible configurational space. The TI technique presented in this article is free of all these limitations.

5   Outlook

Considering the focus of recent studies on adsorption[12,13,127] and on the degree of anharmonicity in solid materials,[128] our contribution advances the field of computational catalysis tremendously: the necessity of accurate free energy calculations beyond the static approach has already been well documented for reaction energetics[3,34,36,129] and our simulation method will enable to achieve a similar level of accuracy also for adsorption problems, which are almost always important parts of catalytic cycles. Several strategies potentially improving the

quality and effectiveness of sampling or accuracy of calculations will be addressed in our future work. First, a more sophisticated choice of the reference Hessian matrix renormalized so as to effectively describe as large part of the anharmonicity of the system as possible would allow to minimize the $\Delta A_{0,q\to1}$ term computed via the TI approach, which would consequently result in faster convergence of the $\langle V_1 - V_{0,q}\rangle_\lambda$ term. In this respect, the ideas beyond the quasi-harmonic approach[117] appear to be very promising. Second, the performance of the TI method could benefit from the use of sophisticated universal coordinates such as descriptors commonly used in the machine learning (ML) community (SOAP,[97] components of Ewald sum (Coulomb) matrices[98]). The use of such coordinates should be explored with regard to their applicability and sampling efficiency. Third, the simulation times necessary to obtain well converged integrands $\langle V_1 - V_{0,q}\rangle_\lambda$ are very long even for the relatively simple adsorption problems discussed in this work. This problem can be alleviated by combining the MD simulations with ML algorithms. Among the most promising approaches in this regard is the seamless ML method of Jinnouchi et al.[130] available in the 6th version of VASP, which is able to learn the underlying model on-the-fly during a DFT-based MD run whereby the model gradually takes control over the simulation while maintaining a controllable error estimation of the ML model. Such a treatment has been shown to accelerate the MD by a factor 300-1000. Finally, the TI method can, in principle, be extended to determine activation free energies via constrained MD without the necessity to sample whole transformation paths (reaction coordinates). Such an approach, if successful, would largely eliminate the problems with various reactions that occur when ionic degrees of freedom are excited.[34,36]

6 Appendix

6.1 VASP keywords and files related to the TI method

The method presented in this work is available in version 6 of VASP. Apart from the usual NVT MD setting, the following parameters and files have to be defined.

TILAMBDA: INCAR flag used to define λ from eq. 4.

HESSEMAT: file defining the Hessian matrix.

ICONST: file defining the coordinates $\boldsymbol{q}$ used in TI calculations.

REPORT: output file that contains the values $\cancel{V_0}$ $V_{0,\boldsymbol{q}}$ and V_1 needed in eq. 6.

Acknowledgement

Supporting Information Available

Free energy contributions by classical and quantum harmonic approximation. Modification of the Hessian matrix eigenspectrum. Computational details and error estimation. Experimental adsorption free energies. Practical information.

This information is available free of charge via the Internet at `http://pubs.acs.org`.

References

(1) Nørskov, J. K.; Studt, F.; Abild-Pedersen, F.; Bligaard, T. *Fundamental Concepts in Heterogeneous Catalysis*; Wiley: Hoboken, New Jersey, 2014.

(2) Bucko, T.; Hafner, J. Entropy Effects in Hydrocarbon Conversion Reactions: Free-Energy Integrations and Transition-Path Sampling. *J. Phys.: Condens. Matter* **2010**, *22*, 384201.

(3) Bučko, T.; Benco, L.; Hafner, J.; Ángyán, J. G. Monomolecular Cracking of Propane over Acidic Chabazite: An Ab Initio Molecular Dynamics and Transition Path Sampling Study. *J. Catal.* **2011**, *279*, 220–228.

(4) Rey, J.; Gomez, A.; Raybaud, P.; Chizallet, C.; Bučko, T. On the Origin of the Difference between Type A and Type B Skeletal Isomerization of Alkenes Catalyzed by Zeolites: The Crucial Input of Ab Initio Molecular Dynamics. *J. Catal.* **2019**, *373*, 361–373.

(5) Cramer, C. J. *Essentials of Computational Chemistry: Theories and Models*, 2nd ed.; Wiley: Chichester, West Sussex, England ; Hoboken, NJ, 2004.

(6) Pitt, I. G.; Gilbert, R. G.; Ryan, K. R. Application of Transition-State Theory to Gas-Surface Reactions: Barrierless Adsorption on Clean Surfaces. *J. Phys. Chem.* **1994**, *98*, 13001–13010.

(7) Campbell, C. T.; Sellers, J. R. V. The Entropies of Adsorbed Molecules. *J. Am. Chem. Soc.* **2012**, *134*, 18109–18115.

(8) Campbell, C. T.; Árnadóttir, L.; Sellers, J. R. V. Kinetic Prefactors of Reactions on Solid Surfaces. *Z. Phys. Chem.* **2013**, *227*.

(9) Campbell, C. T.; Sprowl, L. H.; Árnadóttir, L. Equilibrium Constants and Rate Con-

stants for Adsorbates: Two-Dimensional (2D) Ideal Gas, 2D Ideal Lattice Gas, and Ideal Hindered Translator Models. *J. Phys. Chem. C* **2016**, *120*, 10283–10297.

(10) Paolucci, C.; Verma, A. A.; Bates, S. A.; Kispersky, V. F.; Miller, J. T.; Gounder, R.; Delgass, W. N.; Ribeiro, F. H.; Schneider, W. F. Isolation of the Copper Redox Steps in the Standard Selective Catalytic Reduction on Cu-SSZ-13. *Angew. Chem. Int. Ed.* **2014**, *53*, 11828–11833.

(11) Dauenhauer, P. J.; Abdelrahman, O. A. A Universal Descriptor for the Entropy of Adsorbed Molecules in Confined Spaces. *ACS Cent. Sci.* **2018**, *4*, 1235–1243.

(12) Bajpai, A.; Mehta, P.; Frey, K.; Lehmer, A. M.; Schneider, W. F. Benchmark First-Principles Calculations of Adsorbate Free Energies. *ACS Catal.* **2018**, *8*, 1945–1954.

(13) Réocreux, R.; Michel, C.; Fleurat-Lessard, P.; Sautet, P.; Steinmann, S. N. Evaluating Thermal Corrections for Adsorption Processes at the Metal/Gas Interface. *J. Phys. Chem. C* **2019**, *123*, 28828–28835.

(14) Piccini, G.; Alessio, M.; Sauer, J. *Ab Initio* Study of Methanol and Ethanol Adsorption on Brønsted Sites in Zeolite H-MFI. *Phys. Chem. Chem. Phys.* **2018**, *20*, 19964–19970.

(15) Alexopoulos, K.; Lee, M.-S.; Liu, Y.; Zhi, Y.; Liu, Y.; Reyniers, M.-F.; Marin, G. B.; Glezakou, V.-A.; Rousseau, R.; Lercher, J. A. Anharmonicity and Confinement in Zeolites: Structure, Spectroscopy, and Adsorption Free Energy of Ethanol in H-ZSM-5. *J. Phys. Chem. C* **2016**, *120*, 7172–7182.

(16) Piccini, G.; Sauer, J. Quantum Chemical Free Energies: Structure Optimization and Vibrational Frequencies in Normal Modes. *J. Chem. Theory Comput.* **2013**, *9*, 5038–5045.

(17) Piccini, G.; Sauer, J. Effect of Anharmonicity on Adsorption Thermodynamics. *J. Chem. Theory Comput.* **2014**, *10*, 2479–2487.

(18) Piccini, G.; Alessio, M.; Sauer, J.; Zhi, Y.; Liu, Y.; Kolvenbach, R.; Jentys, A.; Lercher, J. A. Accurate Adsorption Thermodynamics of Small Alkanes in Zeolites. Ab Initio Theory and Experiment for H-Chabazite. *J. Phys. Chem. C* **2015**, *119*, 6128–6137.

(19) Piccini, G.; Alessio, M.; Sauer, J. Ab Initio Calculation of Rate Constants for Molecule-Surface Reactions with Chemical Accuracy. *Angew. Chem. Int. Ed.* **2016**, *55*, 5235–5237.

(20) Kundu, A.; Piccini, G.; Sillar, K.; Sauer, J. Ab Initio Prediction of Adsorption Isotherms for Small Molecules in Metal–Organic Frameworks. *J. Am. Chem. Soc.* **2016**, *138*, 14047–14056.

(21) Pitzer, K. S.; Gwinn, W. D. Energy Levels and Thermodynamic Functions for Molecules with Internal Rotation I. Rigid Frame with Attached Tops. *J. Chem. Phys.* **1942**, *10*, 428–440.

(22) McClurg, R. B.; Flagan, R. C.; Goddard III, W. A. The Hindered Rotor Density-of-States Interpolation Function. *J. Chem. Phys.* **1997**, *106*, 6675–6680.

(23) Sprowl, L. H.; Campbell, C. T.; Árnadóttir, L. Hindered Translator and Hindered Rotor Models for Adsorbates: Partition Functions and Entropies. *J. Phys. Chem. C* **2016**, *120*, 9719–9731.

(24) Pfaendtner, J.; Yu, X.; Broadbelt, L. J. The 1-D Hindered Rotor Approximation. *Theor. Chem. Acc.* **2007**, *118*, 881–898.

(25) Jørgensen, M.; Grönbeck, H. Adsorbate Entropies with Complete Potential Energy Sampling in Microkinetic Modeling. *J. Phys. Chem. C* **2017**, *121*, 7199–7207.

(26) Van Speybroeck, V.; Van Neck, D.; Waroquier, M.; Wauters, S.; Saeys, M.;

Marin, G. B. Ab Initio Study of Radical Addition Reactions: Addition of a Primary Ethylbenzene Radical to Ethene (I). *J. Phys. Chem. A* **2000**, *104*, 10939–10950.

(27) Van Speybroeck, V.; Van Neck, D.; Waroquier, M. Ab Initio Study of Radical Reactions: Role of Coupled Internal Rotations on the Reaction Kinetics (III). *J. Phys. Chem. A* **2002**, *106*, 8945–8950.

(28) Vansteenkiste, P.; Van Speybroeck, V.; Marin, G. B.; Waroquier, M. Ab Initio Calculation of Entropy and Heat Capacity of Gas-Phase n -Alkanes Using Internal Rotations. *J. Phys. Chem. A* **2003**, *107*, 3139–3145.

(29) Carter, E. A.; Ciccotti, G.; Hynes, J. T.; Kapral, R. Constrained Reaction Coordinate Dynamics for the Simulation of Rare Events. *Chem. Phys. Lett.* **1989**, *156*, 472–477.

(30) Ciccotti, G.; Kapral, R.; Vanden-Eijnden, E. Blue Moon Sampling, Vectorial Reaction Coordinates, and Unbiased Constrained Dynamics. *ChemPhysChem* **2005**, *6*, 1809–1814.

(31) Torrie, G. M.; Valleau, J. P. Monte Carlo Free Energy Estimates Using Non-Boltzmann Sampling: Application to the Sub-Critical Lennard-Jones Fluid. *Chem. Phys. Lett.* **1974**, *28*, 578–581.

(32) Torrie, G.; Valleau, J. Nonphysical Sampling Distributions in Monte Carlo Free-Energy Estimation: Umbrella Sampling. *J. Comput. Chem.* **1977**, *23*, 187–199.

(33) Kästner, J. Umbrella Sampling: Umbrella Sampling. *Wires Comput. Mol. Sci.* **2011**, *1*, 932–942.

(34) Rey, J.; Raybaud, P.; Chizallet, C.; Bučko, T. Competition of Secondary versus Tertiary Carbenium Routes for the Type B Isomerization of Alkenes over Acid Zeolites Quantified by Ab Initio Molecular Dynamics Simulations. *ACS Catal.* **2019**, *9*, 9813–9828.

(35) Cnudde, P.; De Wispelaere, K.; Van der Mynsbrugge, J.; Waroquier, M.; Van Spey-broeck, V. Effect of Temperature and Branching on the Nature and Stability of Alkene Cracking Intermediates in H-ZSM-5. *J. Catal.* **2017**, *345*, 53–69.

(36) Cnudde, P.; De Wispelaere, K.; Vanduyfhuys, L.; Demuynck, R.; Van der Myns-brugge, J.; Waroquier, M.; Van Speybroeck, V. How Chain Length and Branching Influence the Alkene Cracking Reactivity on H-ZSM-5. *ACS Catal.* **2018**, *8*, 9579–9595.

(37) Bailleul, S.; Rogge, S. M. J.; Vanduyfhuys, L.; Van Speybroeck, V. Insight into the Role of Water on the Methylation of Hexamethylbenzene in H-SAPO-34 from First Principle Molecular Dynamics Simulations. *ChemCatChem* **2019**, *11*, 3993–4010.

(38) Bailleul, S.; Dedecker, K.; Cnudde, P.; Vanduyfhuys, L.; Waroquier, M.; Van Spey-broeck, V. Ab Initio Enhanced Sampling Kinetic Study on MTO Ethene Methylation Reaction. *J. Catal.* **2020**, *388*, 38–51.

(39) Li, H.; Paolucci, C.; Schneider, W. F. Zeolite Adsorption Free Energies from Ab Initio Potentials of Mean Force. *J. Chem. Theory Comput.* **2018**, *14*, 929–938.

(40) Beveridge, D. L.; DiCapua, F. M. Free Energy Via Molecular Simulation: Applications to Chemical and Biomolecular Systems. *Annu. Rev. Biophys. Biophys. Chem.* **1989**, *18*, 431–492.

(41) Frenkel, D.; Smit, B. *Understanding Molecular Simulation: From Algorithms to Applications*, 2nd ed.; Computational Science Series 1; Academic Press: San Diego, 2002.

(42) Chipot, C., Pohorille, A., Eds. *Free Energy Calculations: Theory and Applications in Chemistry and Biology*; Springer Series in Chemical Physics 86; Springer: Berlin; New York, 2007.

(43) Straatsma, T. P.; Berendsen, H. J. C. Free Energy of Ionic Hydration: Analysis of a Thermodynamic Integration Technique to Evaluate Free Energy Differences by Molecular Dynamics Simulations. *J. Chem. Phys.* **1988**, *89*, 5876–5886.

(44) de Oliveira, C. A. F.; Hamelberg, D.; McCammon, J. A. Coupling Accelerated Molecular Dynamics Methods with Thermodynamic Integration Simulations. *J. Chem. Theory Comput.* **2008**, *4*, 1516–1525.

(45) Leroy, F.; dos Santos, D. J. V. A.; Müller-Plathe, F. Interfacial Excess Free Energies of Solid-Liquid Interfaces by Molecular Dynamics Simulation and Thermodynamic Integration. *Macromol. Rapid Commun.* **2009**, *30*, 864–870.

(46) Pohorille, A.; Jarzynski, C.; Chipot, C. Good Practices in Free-Energy Calculations. *J. Phys. Chem. B* **2010**, *114*, 10235–10253.

(47) Bruckner, S.; Boresch, S. Efficiency of Alchemical Free Energy Simulations. II. Improvements for Thermodynamic Integration. *J. Comput. Chem.* **2011**, *32*, 1320–1333.

(48) de Ruiter, A.; Oostenbrink, C. Efficient and Accurate Free Energy Calculations on Trypsin Inhibitors. *J. Chem. Theory Comput.* **2012**, *8*, 3686–3695.

(49) Moustafa, S. G.; Schultz, A. J.; Kofke, D. A. Very Fast Averaging of Thermal Properties of Crystals by Molecular Simulation. *Phys. Rev. E* **2015**, *92*, 043303.

(50) Moustafa, S. G.; Schultz, A. J.; Kofke, D. A. Harmonically Assisted Methods for Computing the Free Energy of Classical Crystals by Molecular Simulation: A Comparative Study. *J. Chem. Theory Comput.* **2017**, *13*, 825–834.

(51) Vočadlo, L.; Alfè, D. *Ab Initio* Melting Curve of the Fcc Phase of Aluminum. *Phys. Rev. B* **2002**, *65*, 214105.

(52) Grabowski, B.; Ismer, L.; Hickel, T.; Neugebauer, J. *Ab Initio* up to the Melting Point: Anharmonicity and Vacancies in Aluminum. *Phys. Rev. B* **2009**, *79*, 134106.

(53) Hellman, O.; Abrikosov, I. A.; Simak, S. I. Lattice Dynamics of Anharmonic Solids from First Principles. *Phys. Rev. B* **2011**, *84*, 180301.

(54) Glensk, A.; Grabowski, B.; Hickel, T.; Neugebauer, J. Breakdown of the Arrhenius Law in Describing Vacancy Formation Energies: The Importance of Local Anharmonicity Revealed by *Ab Initio* Thermodynamics. *Phys. Rev. X* **2014**, *4*, 011018.

(55) Glensk, A.; Grabowski, B.; Hickel, T.; Neugebauer, J. Understanding Anharmonicity in Fcc Materials: From Its Origin to *Ab Initio* Strategies beyond the Quasiharmonic Approximation. *Phys. Rev. Lett.* **2015**, *114*, 195901.

(56) Duff, A. I.; Davey, T.; Korbmacher, D.; Glensk, A.; Grabowski, B.; Neugebauer, J.; Finnis, M. W. Improved Method of Calculating *Ab Initio* High-Temperature Thermodynamic Properties with Application to ZrC. *Phys. Rev. B* **2015**, *91*, 214311.

(57) Jinnouchi, R.; Karsai, F.; Kresse, G. Making Free-Energy Calculations Routine: Combining First Principles with Machine Learning. *Phys. Rev. B* **2020**, *101*, 060201.

(58) Habershon, S.; Manolopoulos, D. E. Free Energy Calculations for a Flexible Water Model. *Phys. Chem. Chem. Phys.* **2011**, *13*, 19714.

(59) Rossi, M.; Gasparotto, P.; Ceriotti, M. Anharmonic and Quantum Fluctuations in Molecular Crystals: A First-Principles Study of the Stability of Paracetamol. *Phys. Rev. Lett.* **2016**, *117*, 115702.

(60) Wilson, E. B.; Decius, J. C.; Cross, P. C. *Molecular Vibrations: The Theory of Infrared and Raman Vibrational Spectra*; Dover Publications: New York, 1980.

(61) Barrer, R. M.; Davies, J. A. Sorption in Decationated Zeolites. I. Gases in Hydrogen-Chabazite. *Proc. Roy. Soc. Lond. A.* **1970**, *320*, 289–308.

(62) Stroud, H. J. F.; Richards, E.; Limcharoen, P.; Parsonage, N. G. Thermodynamic

Study of the Linde Sieve 5A + Methane System. *J. Chem. Soc., Faraday Trans. 1* **1976**, *72*, 942.

(63) Soto, J.; Myers, A. Monte Carlo Studies of Adsorption in Molecular Sieves. *Mol. Phys.* **1981**, *42*, 971–983.

(64) Woods, G. B.; Rowlinson, J. S. Computer Simulations of Fluids in Zeolites X and Y. *J. Chem. Soc., Faraday Trans. 2* **1989**, *85*, 765.

(65) Snurr, R. Q.; June, R. L.; Bell, A. T.; Theodorou, D. N. Molecular Simulations of Methane Adsorption in Silicalite. *Mol. Simulat.* **1991**, *8*, 73–92.

(66) Karavias, F.; Myers, A. L. Isosteric Heats of Multicomponent Adsorption: Thermodynamics and Computer Simulations. *Langmuir* **1991**, *7*, 3118–3126.

(67) Catlow, C. R. A., Ed. *Modelling of Structure and Reactivity in Zeolites*; Acad. Press: London, 1992.

(68) Van Tassel, P. R.; Davis, H. T.; McCormick, A. V. Open-system Monte Carlo Simulations of Xe in NaA. *J. Chem. Phys.* **1993**, *98*, 8919–8928.

(69) Maddox, M. W.; Rowlinson, J. S. Computer Simulation of the Adsorption of a Fluid Mixture in Zeolite Y. *Faraday Trans.* **1993**, *89*, 3619.

(70) Smit, B. Simulating the Adsorption Isotherms of Methane, Ethane, and Propane in the Zeolite Silicalite. *J. Phys. Chem.* **1995**, *99*, 5597–5603.

(71) Bučko, T.; Hafner, J. The Role of Spatial Constraints and Entropy in the Adsorption and Transformation of Hydrocarbons Catalyzed by Zeolites. *J. Catal.* **2015**, *329*, 32–48.

(72) Moustafa, S. G.; Schultz, A. J.; Kofke, D. A. A Comparative Study of Methods to Compute the Free Energy of an Ordered Assembly by Molecular Simulation. *J. Chem. Phys.* **2013**, *139*, 084105.

(73) Moustafa, S. G.; Schultz, A. J.; Kofke, D. A. Effects of Thermostatting in Molecular Dynamics on Anharmonic Properties of Crystals: Application to Fcc Al at High Pressure and Temperature. *J. Chem. Phys.* **2018**, *149*, 124109.

(74) Purohit, A.; Schultz, A. J.; Moustafa, S. G.; Errington, J. R.; Kofke, D. A. Free Energy and Concentration of Crystalline Vacancies by Molecular Simulation. *Mol. Phys.* **2018**, *116*, 3027–3041.

(75) Moustafa, S. G.; Purohit, A.; Schultz, A. J.; Kofke, D. A. pyHMA: A VASP Post-Processor for Precise Measurement of Crystalline Anharmonic Properties Using Harmonically Mapped Averaging. *Comput. Phys. Commun.* **2021**, *258*, 107554.

(76) De Moor, B. A.; Ghysels, A.; Reyniers, M.-F.; Van Speybroeck, V.; Waroquier, M.; Marin, G. B. Normal Mode Analysis in Zeolites: Toward an Efficient Calculation of Adsorption Entropies. *J. Chem. Theory Comput.* **2011**, *7*, 1090–1101.

(77) Uzunova, E. L.; Mikosch, H. Adsorption and Activation of Ethene in Transition Metal Exchanged Zeolite Clinoptilolite: A Density Functional Study. *ACS Catal.* **2013**, *3*, 2759–2767.

(78) Wang, C.-M.; Brogaard, R. Y.; Xie, Z.-K.; Studt, F. Transition-State Scaling Relations in Zeolite Catalysis: Influence of Framework Topology and Acid-Site Reactivity. *Catal. Sci. Technol.* **2015**, *5*, 2814–2820.

(79) De Moor, B. A.; Reyniers, M.-F.; Gobin, O. C.; Lercher, J. A.; Marin, G. B. Adsorption of C2-C8 n-Alkanes in Zeolites. *J. Phys. Chem. C* **2011**, *115*, 1204–1219.

(80) Su, Y.-Q.; Wang, Y.; Liu, J.-X.; Filot, I. A.; Alexopoulos, K.; Zhang, L.; Muravev, V.; Zijlstra, B.; Vlachos, D. G.; Hensen, E. J. Theoretical Approach To Predict the Stability of Supported Single-Atom Catalysts. *ACS Catal.* **2019**, *9*, 3289–3297.

(81) Tuckerman, M. E. *Statistical Mechanics: Theory and Molecular Simulation*; Oxford University Press: Oxford ; New York, 2010.

(82) Jensen, F. *Introduction to Computational Chemistry*, 2nd ed.; John Wiley & Sons: Chichester, England ; Hoboken, NJ, 2007.

(83) Wilson, E. B. Some Mathematical Methods for the Study of Molecular Vibrations. *J. Chem. Phys.* **1941**, *9*, 76–84.

(84) Fogarasi, G.; Zhou, X.; Taylor, P. W.; Pulay, P. The Calculation of Ab Initio Molecular Geometries: Efficient Optimization by Natural Internal Coordinates and Empirical Correction by Offset Forces. *J. Am. Chem. Soc.* **1992**, *114*, 8191–8201.

(85) Baker, J. Techniques for Geometry Optimization: A Comparison of Cartesian and Natural Internal Coordinates. *J. Comput. Chem.* **1993**, *14*, 1085–1100.

(86) Bakken, V.; Helgaker, T. The Efficient Optimization of Molecular Geometries Using Redundant Internal Coordinates. *J. Chem. Phys.* **2002**, *117*, 9160–9174.

(87) Bučko, T.; Hafner, J.; Ángyán, J. G. Geometry Optimization of Periodic Systems Using Internal Coordinates. *J. Chem. Phys.* **2005**, *122*, 124508.

(88) Bučko, T. Transition State Optimization of Periodic Systems Using Delocalized Internal Coordinates. *Theor. Chem. Acc.* **2018**, *137*, 164.

(89) Sprik, M. Coordination Numbers as Reaction Coordinates in Constrained Molecular Dynamics. *Faraday Disc.* **1998**, *110*, 437–445.

(90) Pulay, P.; Fogarasi, G.; Pang, F.; Boggs, J. E. Systematic Ab Initio Gradient Calculation of Molecular Geometries, Force Constants, and Dipole Moment Derivatives. *J. Am. Chem. Soc.* **1979**, *101*, 2550–2560.

(91) Pulay, P.; Fogarasi, G. Geometry Optimization in Redundant Internal Coordinates. *J. Chem. Phys.* **1992**, *96*, 2856–2860.

(92) Baker, J.; Kessi, A.; Delley, B. The Generation and Use of Delocalized Internal Coordinates in Geometry Optimization. *J. Chem. Phys.* **1996**, *105*, 192–212.

(93) Peng, C.; Ayala, P. Y.; Schlegel, H. B.; Frisch, M. J. Using Redundant Internal Coordinates to Optimize Equilibrium Geometries and Transition States. *J. Comput. Chem.* **1996**, *17*, 49–56.

(94) Andzelm, J.; King-Smith, R.; Fitzgerald, G. Geometry Optimization of Solids Using Delocalized Internal Coordinates. *Chem. Phys. Lett.* **2001**, *335*, 321–326.

(95) Kudin, K. N.; Scuseria, G. E.; Schlegel, H. B. A Redundant Internal Coordinate Algorithm for Optimization of Periodic Systems. *J. Chem. Phys.* **2001**, *114*, 2919–2923.

(96) Panosetti, C.; Krautgasser, K.; Palagin, D.; Reuter, K.; Maurer, R. J. Global Materials Structure Search with Chemically Motivated Coordinates. *Nano Lett.* **2015**, *15*, 8044–8048.

(97) Bartók, A. P.; Kondor, R.; Csányi, G. On Representing Chemical Environments. *Phys. Rev. B* **2013**, *87*, 184115.

(98) Rupp, M.; Tkatchenko, A.; Müller, K.-R.; von Lilienfeld, O. A. Fast and Accurate Modeling of Molecular Atomization Energies with Machine Learning. *Phys. Rev. Lett.* **2012**, *108*, 058301.

(99) Jablonka, K. M.; Ongari, D.; Moosavi, S. M.; Smit, B. Big-Data Science in Porous Materials: Materials Genomics and Machine Learning. *Chem. Rev.* **2020**, *120*, 8066–8129.

(100) Kresse, G.; Hafner, J. *Ab Initio* Molecular Dynamics for Open-Shell Transition Metals. *Phys. Rev. B* **1993**, *48*, 13115–13118.

(101) Kresse, G.; Hafner, J. *Ab Initio* Molecular-Dynamics Simulation of the Liquid-Metal–Amorphous-Semiconductor Transition in Germanium. *Phys. Rev. B* **1994**, *49*, 14251–14269.

(102) Kresse, G.; Furthmüller, J. Efficiency of Ab-Initio Total Energy Calculations for Metals and Semiconductors Using a Plane-Wave Basis Set. *Comput. Mater. Sci.* **1996**, *6*, 15–50.

(103) Kresse, G.; Furthmüller, J. Efficient Iterative Schemes for *Ab Initio* Total-Energy Calculations Using a Plane-Wave Basis Set. *Phys. Rev. B* **1996**, *54*, 11169–11186.

(104) Blöchl, P. E. Projector Augmented-Wave Method. *Phys. Rev. B* **1994**, *50*, 17953–17979.

(105) Kresse, G.; Joubert, D. From Ultrasoft Pseudopotentials to the Projector Augmented-Wave Method. *Phys. Rev. B* **1999**, *59*, 1758–1775.

(106) Perdew, J. P.; Burke, K.; Ernzerhof, M. Generalized Gradient Approximation Made Simple. *Phys. Rev. Lett.* **1996**, *77*, 3865–3868.

(107) Grimme, S.; Antony, J.; Ehrlich, S.; Krieg, H. A Consistent and Accurate *Ab Initio* Parametrization of Density Functional Dispersion Correction (DFT-D) for the 94 Elements H-Pu. *J. Chem. Phys.* **2010**, *132*, 154104.

(108) Bučko, T.; Hafner, J.; Lebègue, S.; Ángyán, J. G. Improved Description of the Structure of Molecular and Layered Crystals: Ab Initio DFT Calculations with van Der Waals Corrections. *J. Phys. Chem. A* **2010**, *114*, 11814–11824.

(109) Monkhorst, H. J.; Pack, J. D. Special Points for Brillouin-Zone Integrations. *Phys. Rev. B* **1976**, *13*, 5188–5192.

(110) Andersen, H. C. Molecular Dynamics Simulations at Constant Pressure and/or Temperature. *J. Chem. Phys.* **1980**, *72*, 2384–2393.

(111) Schiferl, S. K.; Wallace, D. C. Statistical Errors in Molecular Dynamics Averages. *J. Chem. Phys.* **1985**, *83*, 5203–5209.

(112) Shklov, N. Simpson's Rule for Unequally Spaced Ordinates. *Am. Math. Mon.* **1960**, *67*, 1022.

(113) Press, W. H., Ed. *Numerical Recipes: The Art of Scientific Computing*, 3rd ed.; Cambridge University Press: Cambridge, UK; New York, 2007.

(114) Cameron, R., B. Numerically Integrating Irregularly-Spaced (x, y) Data. *Math. Enthus.* **2014**, *11*.

(115) Flyvbjerg, H.; Petersen, H. G. Error Estimates on Averages of Correlated Data. *J. Chem. Phys.* **1989**, *91*, 461–466.

(116) Irikura, K. K. Experimental Vibrational Zero-Point Energies: Diatomic Molecules. *J. Phys. Chem. Ref. Data* **2007**, *36*, 389–397.

(117) Baron, R.; van Gunsteren, W.; Hünenberger, P. Estimating the Configurational Entropy from Molecular Dynamics Simulations: Anharmonicity and Correlation Corrections to the Quasi-Harmonic Approximation. *Trends Phys. Chem.* **2006**, *11*, 87–122.

(118) Baron, R.; Hünenberger, P. H.; McCammon, J. A. Absolute Single-Molecule Entropies from Quasi-Harmonic Analysis of Microsecond Molecular Dynamics: Correction Terms and Convergence Properties. *J. Chem. Theory Comput.* **2009**, *5*, 3150–3160.

(119) Jeanvoine, Y.; Ángyán, J. G.; Kresse, G.; Hafner, J. Brønsted Acid Sites in HSAPO-34 and Chabazite: An Ab Initio Structural Study. *J. Phys. Chem. B* **1998**, *102*, 5573–5580.

(120) Smith, L.; Davidson, A.; Cheetham, A. A Neutron Diffraction and Infrared Spectroscopy Study of the Acid Form of the Aluminosilicate Zeolite, Chabazite (H-SSZ-13). *Catal. Lett.* **1997**, *49*, 143–146.

(121) Berens, P. H.; Mackay, D. H. J.; White, G. M.; Wilson, K. R. Thermodynamics and Quantum Corrections from Molecular Dynamics for Liquid Water. *J. Chem. Phys.* **1983**, *79*, 2375–2389.

(122) Hoover, W. G.; Ladd, A. J. C.; Moran, B. High-Strain-Rate Plastic Flow Studied via Nonequilibrium Molecular Dynamics. *Phys. Rev. Lett.* **1982**, *48*, 1818–1820.

(123) Evans, D. J. Computer "Experiment" for Nonlinear Thermodynamics of Couette Flow. *J. Chem. Phys.* **1983**, *78*, 3297–3302.

(124) Nosé, S. A Unified Formulation of the Constant Temperature Molecular Dynamics Methods. *J. Chem. Phys.* **1984**, *81*, 511–519.

(125) Hoover, W. G. Canonical Dynamics: Equilibrium Phase-Space Distributions. *Phys. Rev. A* **1985**, *31*, 1695–1697.

(126) Martyna, G. J.; Klein, M. L.; Tuckerman, M. Nosé–Hoover Chains: The Canonical Ensemble via Continuous Dynamics. *J. Chem. Phys.* **1992**, *97*, 2635–2643.

(127) Collinge, G.; Yuk, S. F.; Nguyen, M.-T.; Lee, M.-S.; Glezakou, V.-A.; Rousseau, R. Effect of Collective Dynamics and Anharmonicity on Entropy in Heterogenous Catalysis: Building the Case for Advanced Molecular Simulations. *ACS Catal.* **2020**, *10*, 9236–9260.

(128) Knoop, F.; Purcell, T. A. R.; Scheffler, M.; Carbogno, C. Anharmonicity Measure for Materials. *Phys. Rev. Materials* **2020**, *4*, 083809.

(129) Van Speybroeck, V.; De Wispelaere, K.; Van der Mynsbrugge, J.; Vandichel, M.; Hemelsoet, K.; Waroquier, M. First Principle Chemical Kinetics in Zeolites: The Methanol-to-Olefin Process as a Case Study. *Chem. Soc. Rev.* **2014**, *43*, 7326–7357.

(130) Jinnouchi, R.; Lahnsteiner, J.; Karsai, F.; Kresse, G.; Bokdam, M. Phase Transitions

of Hybrid Perovskites Simulated by Machine-Learning Force Fields Trained on the Fly with Bayesian Inference. *Phys. Rev. Lett.* **2019**, *122*, 225701.

Graphical TOC Entry